Geophysical And Astrophysical Fluid Dynamics
November 2021, Volume 115 Issue 5-6 Pages 523-550
https://doi.org/10.1080/03091929.2021.1881780
https://archimer.ifremer.fr/doc/00816/92801/

The merger of two three-dimensional quasi-geostrophic baroclinic tripolar eddies

Reinaud Jean N. [1, *], Carton Xavier [2]

[1] School of Mathematics and Statistics, University of St Andrews, St Andrews, UK;
[2] LOPS IUEM/UBO, Plouzané, France.

* Corresponding author : Jean N. Reinaud, email address : jnr1@st-andrews.ac.uk

Abstract :

We investigate the strong interaction between two baroclinic tripolar eddies in a three-dimensional, rapidly-rotating, continuously stratified flow under the quasi-geostrophic approximation. Each tripolar eddy consists of an anticyclonic central vortex with two oblate cyclonic vortices located above and below the anticyclone. The interaction depends on the vertical and horizontal offsets between the two tripolar eddies. For small and low PV oblate cyclones, each tripolar eddy alone is only weakly unstable to a baroclinic mode. The instability puts the three vortices out of alignment. Most of the eddy however survives the instability. When two tripolar eddies interact, their constituent vortices may merge. Mergeroccurs when the eddies are close enough together, and shows similarities with the merger of monopolar vortices. Vertically separated eddies do not align vertically. This suggests the importance of an external flow for the alignment, observed in the oceans, to occur. We finally show that the interaction between two tripolar eddies with intense oblate cyclones is very different and show similarities with the dynamics of dipolar baroclinic eddies known as hetons.

Keywords : Quasi-geostrophy, vortex interactions, vortex merger

1. Introduction

We investigate the interaction between two identical mesoscale eddies. Each eddy consists of a central anticyclonic vortex surrounded above and below by smaller and weaker cyclonic lenses. A motivation for the study stems from observations of Mediterranean water Eddies (or Meddies) in the North Atlantic, see e.g. Richardson *et al.* (2000). The stability of various baroclinic eddies has been studied by many authors, including Nguyen *et al.* (2012), Meunier *et al.* (2015), Yim *et al.* (2016), Storer *et al.* (2018), Menesguen *et al.* (2018), Meunier *et al.* (2018), Carton *et al.* (2014) for so-called Gaussian vortices, or for piecewise uniform vortices by Miyazaki *et al.* (2003), Reinaud (2017). On the other hand, tripolar vortices where two like-signed vortices are at the same depth have been investigated by Reinaud and Carton (2015). In the absence of the cyclonic lenses, the strong interaction between two like-signed vortices has already been extensively studied in the literature. One of the possible outcome of such interactions is the vortex merger, whereby the two vortices combine, in general only partially, to form a larger vortex. Vortex merger has often been observed in the oceans. For example, instances of vortex merger has been observed in East Australian current (Cressell, 1982) and in the vicinity of the Kuroshio current (Yasuda, Okuda and Hirai, 1992). More recently the merger of two storms has been observed in the Jovian atmosphere.[1] Vortex merger has also be extensively studied numerically. The merger of two monopolar planar two-dimensional vortices has been investigated by Overman II and Zabusky (1982), Melander *et al.* (1988), Dritschel and Waugh (1992), Waugh (1992), Dritschel (1995) to name but a few studies. The merger of two monopolar three-dimensional vortices in geophysical context has been studied by von

Hardenberg *et al.* (2000), Dritschel (2002), Reinaud and Dritschel (2002, 2005), Bambrey *et al.* (2007), Ozugurlu *et al.* (2008), Reinaud and Dritschel (2018). The upshot of these studies, and many others, is that two vortices may merge provided they are separated by a distance less than a threshold known as the critical merger distance. Conservation of invariants, such as the total energy and the angular impulse implies that the formation of a larger vortex from the merger process must be accompanied by the formation of filamentary and small scale secondary vortices and debris. The strong interaction therefore contributes, in physical space, to both an inverse energy cascade due to the formation of a larger vortex, and to direct enstrophy cascades due to the formation of small scale filaments and debris. Such interactions therefore provides a route for the double energy cascades observed in geostrophic turbulence.

In the present paper, we investigate the interaction between two geophysical eddies in the case the vortices are not monopolar but are rather baroclinic tripolar eddies. Such eddies containing potential vorticity anomalies of both signs have often been observed in the oceans, see for example Yang *et al.* (2019) in the Indian ocean. As mentioned, other examples of eddies with both signs of potential vorticity anomalies include the Mediterranean water Eddies (Meddies), see for example Pingree and Le Cann (1993), Carton (2001), Bashmachnikov and Carton (2012). The tripolar structure of Meddies is also discussed by Paillet *et al.* (1999, 2002), Carton *et al.* (2002). Moreover interactions between Meddies have been observed southwest of Portugal during the SEMANE 2000 experiment, see Carton *et al.* (2010). L'Hégaret *et al.* (2014) also reported the interactions of Meddies. The study of the strong interaction between tripolar baroclinic eddies is therefore of interest. Ciani *et al.* (2016) have recently studied numerically the merger of isolated Gaussian vortices solving the primitive equations. The present paper can be seen as an extension to these results by including the effect of a vertical offset between the two vortices, albeit doing so under a simpler, quasi-geostrophic dynamics.

The paper is organised as follows. The mathematical formulation and the geometry of the problem are described in section 2. We then address the linear stability and the nonlinear evolution of a single eddy in section 3 where we show that the eddies are weakly unstable. The timescale associated with the destabilisation of the eddy is however typically larger than the timescale associated with the strong interaction between the vortices. The interaction between two eddies is studied in section 4. Conclusions are given in section 6.

2. Mathematical formulation and geometry

Large scale oceanic flows are strongly influenced by the rapid background planetary rotation and the stable density stratification. The quasi-geostrophic (QG) model is the simplest dynamical model which takes into account these two effects. In the form used in this study, the QG model derives from an asymptotic expansion of Euler's equations for an adiabatic, rotating, stratified fluid under the Boussinesq approximation. It is strictly valid for $Fr^2 \ll Ro \ll 1$, where $Fr = U/(NH)$ and $Ro = U/(fL)$ are the Froude and Rossby numbers respectively. Here U is a characteristic horizontal velocity scale, L and H are characteristic horizontal and vertical length scales respectively. N is the buoyancy frequency while f is the Coriolis frequency. For simplicity, we take N and f constant, and the physical vertical coordinate is stretched by the constant N/f. It should be noted that $N/f \gg 1$ in most parts of the oceans at mid-latitudes, see Dijkstra (2008). Under these assumptions the flow is completely governed by the evolution of a single scalar quantity, the QG potential vorticity anomaly q, hereinafter referred to as PV for simplicity. PV can be defined from the flow streamfunction φ,

$$q = \frac{\partial^2 \varphi}{\partial x^2} + \frac{\partial^2 \varphi}{\partial y^2} + \frac{\partial \varphi}{\partial z^2}, \tag{1}$$

where the streamfunction φ is defined from the non-divergent geostrophic advective horizontal velocities

$$u = -\frac{\partial \varphi}{\partial y}, \qquad v = \frac{\partial \varphi}{\partial x}. \tag{2}$$

Finally, in absence of adiabatic and frictional effects, PV is materially conserved,

$$\frac{\partial q}{\partial t} + u\frac{\partial q}{\partial x} + v\frac{\partial q}{\partial y} = 0. \tag{3}$$

While the vertical velocity is not zero under the QG approximation, it is too small to contribute to the advection in equation (3). A complete derivation of the QG model can be found in Vallis (2006). It should be noted that equation (1) can be formally inverted under the condition $\varphi(\boldsymbol{x}) \to 0$ as $|\boldsymbol{x}| \to \infty$ as

$$\varphi(\boldsymbol{x}) = -\frac{1}{4\pi} \iiint \frac{q(\boldsymbol{x}')}{|\boldsymbol{x} - \boldsymbol{x}'|} \mathrm{d}^3\boldsymbol{x}'. \tag{4}$$

We investigate the interaction between two eddies. Each eddy consist of three uniform PV vortices: a central vortex surrounded above and below by two lenses. The central vortex is a sphere, in the vertically stretched reference frame, of uniform PV $q_c = -2\pi$. We denote its half-height h_c equal to its horizontal radius r_h. The upper (resp. lower) lens is initially a spheroid with the same horizontal radius r_h as the central vortex and half height h_t (resp. h_b) set to 0.25 r_h. The upper (resp. lower) lens has uniform PV q_t (resp. q_b). We consider two different cases. In the first case, we consider *symmetric* baroclinic tripolar eddies where $q_t = q_b = -0.3q_c = 0.6\pi$. In the second case, we consider *asymmetric* baroclinic tripolar eddies with $q_t = 0.2q_c = 0.4\pi$ and $q_b = -0.3q_c = 0.6\pi$. These choices are motivated by estimates made on Meddies, see Paillet *et al.* (2002), Carton *et al.* (2002).

The strength κ of a given vortex of uniform PV q, half-height h and horizontal radius r is given by $\kappa = (4\pi)^{-1} \iiint_{vortex} q(\boldsymbol{x}) \mathrm{d}^3\boldsymbol{x} = qr^2h/3$. The strength ratio between the central vortex and the top vortex is therefore $q_c h_c/(q_t h_t) = 13.3$ for the symmetric eddies and 20 for the asymmetric eddies.

It should be noted that there is no dynamical asymmetry between cyclonic and anticyclonic vortices under the quasi-geostrophic approximation. Considering a cyclonic central vortex surrounded from above and below by anticyclonic lenses leads to the same conclusions.

These values of PV implicitly set the time scale of the problem. For example, a single sphere of uniform PV q has a turnover period $T_{over} = 6\pi/q$. For each eddy, the centres of the three vortices are initially aligned along the same vertical axis, and the three vortices touch. So at $t = 0$, the central vortex eddy i ($i \in \{1, 2\}$) is centred at (x_c^i, y_c^i, z_c^i), and the centre of the upper (resp. lower) lense is $(x_c^i, y_c^i, z_c^i + h_c + h_t)$ (resp. $(x_c^i, y_c^i, z_c^i - h_c - h_b)$). The two eddies are initially separated in the horizontal direction by $\Delta x \equiv x_c^2(t = 0) - x_c^1(t = 0)$, and in the vertical direction by $\Delta z \equiv z_c^2 - z_c^1$ both taken positive without loss of generality. The general geometry of the problem is summarised in figure 1. The length scale of the problem is set by imposing that the total height occupied by the pair of eddies is $H = \Delta z + 2(h_b + h_c + h_t) = 1$.

Both the linear stability analysis and the nonlinear simulations of the eddies are performed using techniques based on Contour Dynamics. The fluid domain is discretised in the vertical direction by a large number n_l of horizontal layers. In each layer, the contours bounding the uniform PV vortices are discretised by a set of nodes whose velocity is obtained by inversion, via equation (4).

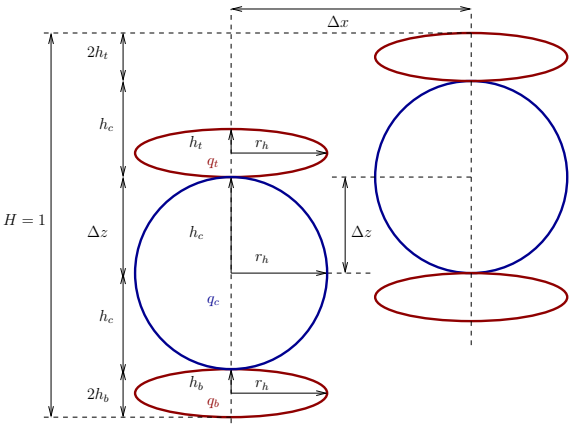

Figure 1. General geometry for two interacting baroclinic tripolar eddies (Colour online).

3. A single baroclinic tripolar eddy

We first investigate the linear stability and the nonlinear evolution of a single baroclinic eddy centred at the origin, $(x_c, y_c, z_c) = (0, 0, 0)$. The PV changes sign in the vertical direction through the tripolar eddy. This means that the tripolar eddy may be sensitive to baroclinic instabilities. Let $\boldsymbol{x}^e = (x_k^e, y_k^e, z_k^e)$ denote the location of a point along a circular contour k bounding the eddy. We analyse deformation modes for the vortex bounding contours by considering radial perturbations of the form

$$r_k' = r_k^e + \frac{\eta_k}{r_k^e} \mathrm{e}^{\sigma t + \mathrm{i}m\theta}, \tag{5}$$

where r_k' is the perturbed (local) horizontal radius of contour k, $r_k^e = \sqrt{x_k^{e\,2} + y_k^{e\,2}}$ is the horizontal radius at equilibrium, η_k is the perturbation 'area', $\sigma \in \mathbb{C}$ is the complex frequency, $m \in \mathbb{R}$ is the azimuthal wave number, $\theta = \tan^{-1}(y/x)$ is the azimuthal angle.

The linearised equation which governs the evolution of the perturbation is

$$\frac{\partial \eta_k}{\partial t} + \Omega_k \frac{\partial \eta_k}{\partial \theta} = \frac{\partial F_k}{\partial \theta} \tag{6}$$

with

$$F_k = \sum_{l=1}^{n_c} \Delta q_l \int_0^{2\pi} \eta_l \mathrm{e}^{\sigma t + \mathrm{i}m\theta'} \, G_{k,l}(|\boldsymbol{x}_k^e(\theta) - \boldsymbol{x}_l^e(\theta')|) \, \mathrm{d}\theta' \tag{7}$$

where $G_{k,l}$ is the Green's function giving the influence of the PV bounded by the contour l on a point along the contour k. Δq_l is the PV jump across the contour l, n_c is the total number of contours, and finally Ω_k is the constant basic-state angular velocity around contour. This leads to a $2 \times n_c$ real eigenvalue problem where σ are the complex eigenvalues and η_k are the eigenvectors.

The real part σ_r of σ corresponds to the growth rate of the mode while the imaginary part, σ_i, is its frequency. It should be noted that of $\sigma = \sigma_r + \mathrm{i}\sigma_i$ is an eigenvalue, it complex conjugate $\sigma^* = \sigma_r - \mathrm{i}\sigma_i$ is also an eigenvalue. Moreover $-\sigma$ and $-\sigma^*$ are also an eigenvalue.

The mode $m = 1$ corresponds to a horizontal shift of the contours, and therefore corresponds to a vertical shearing of the eddy.

For both the symmetric and asymmetric baroclinic tripolar eddies considered in this study,

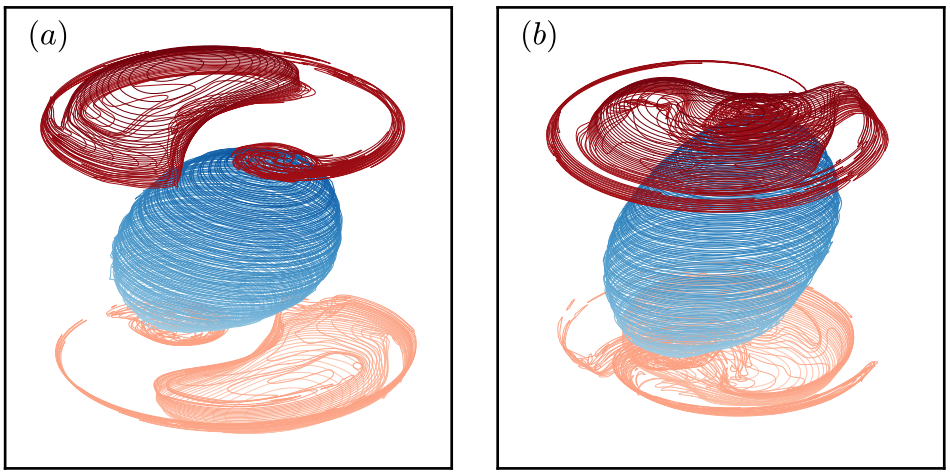

Figure 2. Orthographic view on the vortex bounding contours at $t = 100$ for (a) a symmetric baroclinic tripolar eddy and (b) an asymmetric baroclinic tripolar eddy. The contours are viewed at an angle of 65° from the vertical axis. The colour shading indicates the depth z of the contours, with lighter contours near the bottom. Red contours bound positive (cyclonic) PV, blue contours bound negative (anticyclonic) PV (Colour online).

only the mode $m = 1$ is unstable. The corresponding growth rate is $\sigma_r/q_c = 3.131 \times 10^{-2}$ for the symmetric baroclinic tripolar eddy, and is $\sigma_r/q_c = 2.63 \times 10^{-2}$ for the asymmetric baroclinic tripolar eddy. The growth rate is lower for the asymmetric case compared to the symmetric case because the PV of the top vortex is less in this case, corresponding to a weaker vertical shear.

We next illustrate the effect of the instability on the evolution of the baroclinic tripolar eddies. We perform a nonlinear simulation of a single eddy using Contour Dynamics. Details on the method can be found in Dritschel and Saravanan (1994). The numerical method is purely Lagrangian, and the fluid domain is explicitly infinite. The boundary conditions are that the velocity vanishes at $r = \sqrt{x^2 + y^2 + z^2} \to \infty$. Time is marched using a fourth-order Runge-Kutta scheme with a time-step $\Delta t = \pi/(20q_c)$ for high accuracy. The complexity of the vortex bounding contours is controlled by Contour Surgery, see Dritschel (1988). The full eddy is mapped by $n_l = 203$ horizontal layers in the vertical direction. The surgical parameters are set to standard values: the dimensionless cutoff scale μ is set to 0.15, and the large scale L is set to r_h, see Dritschel (1988) for details. The same surgical scales are used throughout the study.

Figure 2 shows snapshots of the flow at $t = 100$ for both the symmetric and asymmetric baroclinic tripolar eddies. The mode $m = 1$ grows and this growth results in the tilting of the eddies. The three vortices move out of vertical alignment and subsequently deform as the strain and shear induced by the vortices onto each other is no longer axisymmetric. The upper and lower lenses deform more than the central vortex as they contain less intense PV. The ability of a vortex to withstand deformation indeed depends on its PV. Intense (high PV) vortices tend to deform less than weak (low PV) vortices when subject to external strain and shear.

At any time t, we identify the vortices present in the flow as contiguous regions of PV distinguishing regions of positive and negative PV. We can then determine the vortex volumes and the location of their centres by contour integration. The horizontal trajectory of the centres (x_i, y_i, z_i), $i = 1, 2, 3$ of the three largest vortices corresponding respectively to the main part of central vortex and the main parts of the upper and lower lenses is shown in figure $3(a)$ for the symmetric baroclinic tripolar eddy. The centre of the central anticyclonic vortex roughly remains at the origin. On the other hand, the centres of the two upper and lower cyclonic

lenses spiral out until $t \simeq 100$. This is confirmed by the evolution of the horizontal radial distance $\sqrt{x_i^2 + y_i^2}$ of the vortex centres from the $z-$axis in figure 3(b). This indicates that the baroclinic tripolar eddy increasingly tilts as a whole during this time period. Then, the tilting angle of the eddy oscillates as indicated by the oscillation of the radial distance of centres of the upper and lower lenses. Figure 3(c) shows the evolution of the relative volume V/V_0 of the three largest vortices, where V_0 is the volume of each individual vortex at $t = 0$. The largest, central, anticyclonic vortex almost continuously sheds material through small scale filaments and debris. These are produced by the deformation of the central vortex subject to the vertical shear induced by the two lenses, and the associated baroclinic mode $m = 1$. By $t = 200$, which corresponds roughly to 67 vortex turnover periods, the central anticyclonic vortex has lost around 3.5% of its volume. The cyclonic lenses deform more. They however do not shed initially any significant amount of small scale filaments. Instead a large filament forms from both the upper and lower lenses. This filament later detaches from the main lenses at $t \simeq 100$. The evolution of both the upper and the lower lenses is very similar until $t \simeq 110$. Later, due to the build-up of small asymmetries originated in the numerical noise, the filament detaching from the lower cyclonic lens is slightly larger than the filament detaching from the upper lens. This results in a main lower lens being smaller than the upper lens for $t > 110$. Figures 3(d, e, f) show the vortex centres trajectories and their volume evolution for the asymmetric baroclinic tripolar eddy. Results are qualitatively similar. Recall that the growth rate of the baroclinic, vertically-shearing, mode for the asymmetric case is smaller compared to the symmetric case. Consequently, the amplitude of the outward, spiralling motion of the centres of the upper and lower cyclonic lenses is reduced. On the other hand, we see that the weaker upper lens loses more material than the stronger lower lens. The difference is however not significant. Indeed the difference in volume between the upper and lower lenses is of the same order of magnitude as the one observed for the symmetric case, where the asymmetry only originates from numerical noise and the subsequent turbulent-like nature of the flow. In both cases, each lens sheds less than 10% of its volume.

The upshot is that, although the structures are unstable and undergo both deformation and loss of material, the baroclinic tripolar eddies retain most of their volume.

4. Interaction between two baroclinic tripolar eddies

We next investigate the strong interaction between two baroclinic tripolar eddies. We separate the study into two parts due to the lack of vertical advection under the QG approximation. In the first part we consider two eddies vertically offset by $\Delta z/r_h < 3$. Then, the two eddies occupy some common horizontal layers and the eddies can touch (and potentially locally merge). In this regime, we explore three values for the vertical offset, $\Delta z/r_h = 0$, 1.25 and 2.5. For the first two values, the two central anticyclonic vortices share some horizontal layers. On the other hand, in the last case, only the upper cyclonic lens of the lower eddy occupies the same layers as the lower lens of upper eddy. In this case, the two central anticyclonic vortices however cannot merge ($\Delta z > 2r_h = 2h_c$). In a second part we consider $\Delta z/r_h = 3$ and the two eddies do not share common horizontal layers, hence cannot merge convectively. They can still potentially align vertically. The problem of alignment of three-dimensional monopolar vortices under the QG approximation is discussed in detail in Reinaud and Carton (2020).

For each value of the vertical offset Δz, we investigate the influence of the horizontal offset Δx between the two tripolar eddies. In all cases, the interaction is studied numerically using Contour Dynamics. The full vertical extend of the PV distribution $H = 1$ is mapped by 200 layers. Appendix A examines how the numerical method conserves some of the inviscid invariants of QG dynamics.

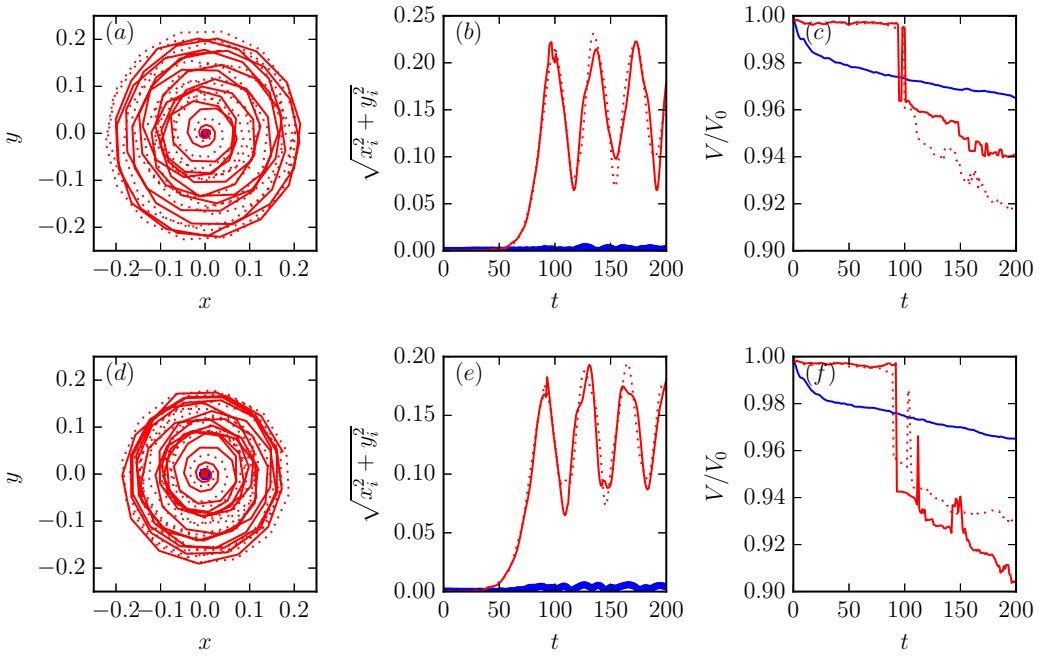

Figure 3. (a) Horizontal trajectories of the centre of the three largest vortices during the nonlinear evolution of the unstable symmetric baroclinic tripolar eddy. (b) Evolution of the horizontal radius $\sqrt{x_i^2+y_i^2}$ of their centres. (c) Evolution of their volume. The blue curves correspond to the central anticyclonic vortex while the red curves correspond to the cyclonic lenses. The solid line corresponds to the upper lens while the dotted line corresponds to the lower lens. (d) same as (a) but for the asymmetric tripolar eddy. (b) same as (e) but for the asymmetric tripolar eddy. (f) same as (d) but for the asymmetric tripolar eddy (Colour online).

4.1. *Moderate vertical offsets*

We first consider the interaction between two tripolar eddies separated in the horizontal direction by $2.1 \leq \Delta x/r_h \leq 3.2$ for the three vertical offsets, $\Delta z/r_h = 0$, 1.25, and 2.5. Simulations are run until $t = 200 \simeq 133\,T_{over}$. T_{over} denotes here the turnover period of a single sphere of uniform PV $q = 2\pi$, equal, in absolute value, to the PV of the spherical central anticyclonic vortex of the tripolar eddies.

As for the single eddy, we identify the coherent structures present in the flow as contiguous regions of PV. We distinguish between regions of negative PV stemming from the two central anticyclones and the regions of positive PV stemming from the cyclonic lenses. We first determine the ratio of the final volume V_f, at $t = 200$, of the two largest anticyclones present in the flow to their initial volume V_0. Results are presented in figure 4. There is overall little qualitative difference between the symmetric and asymmetric configurations. For horizontally aligned eddies, $\Delta z = 0$, the volume of the largest anticyclone formed is larger when the eddies are initially close together, as one expects. In these cases, one of the two anticyclones increases its volume by absorbing material from the other anticyclone through merger. Examples of such close interactions are presented in figure 5 for $\Delta x/r_h = 2.1$ for both the asymmetric and symmetric configurations. The flow snapshots confirm the formation of a main central structure which retains a large part of the total initial negative PV. Small scale debris and filaments are ejected away from the main structure. In the case of the merger of two monopolar vortices, these ejections are associated with the conservation of angular impulse $J = (1/2)\iiint q(x^2+y^2)\mathrm{d}^3\boldsymbol{x}$, see the argument in Reinaud and Carton (2020). A similar ejection occurs here for the tripolar eddies. Conversely, for $\Delta x/r_h < 2.5$, the final volume V_f of the second largest anticyclonic vortex is very small as shown in figure 4(b). This confirms that, besides the largest anticyclone, only small scale anticyclonic debris and filaments remain

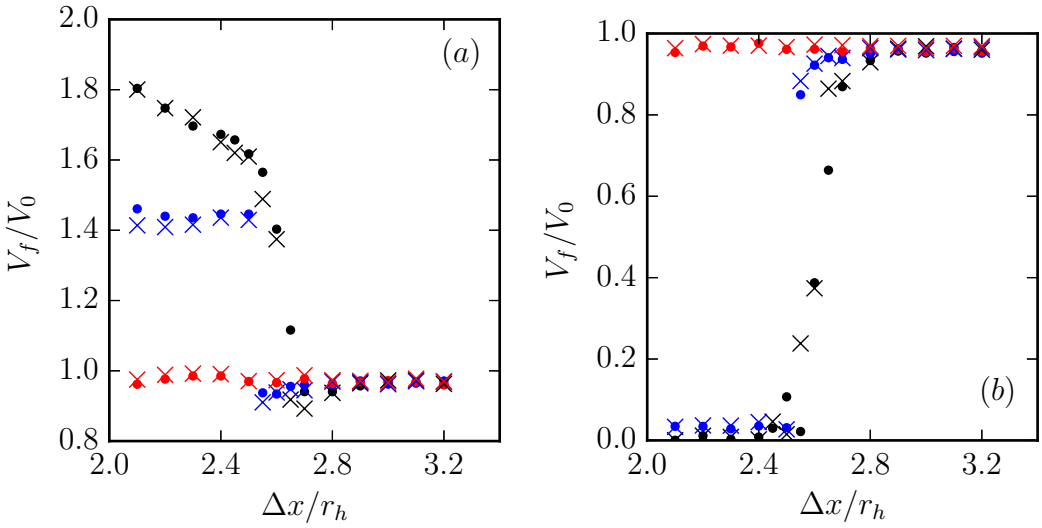

Figure 4. (a) Ratio of the volume at $t = 200$ V_f to the initial volume V_0, of the largest (anticyclonic) vortex present in the flow vs $\Delta x/r_h$ for the asymmetric configuration (•) and symmetric configuration (×) for $\Delta z = 0$ (black), $\Delta z/r_h = 1.25$ (blue) and $\Delta z = 2.5$ (red). (b) V_f/V_0 for the second largest anticyclone (same conventions). (Colour online).

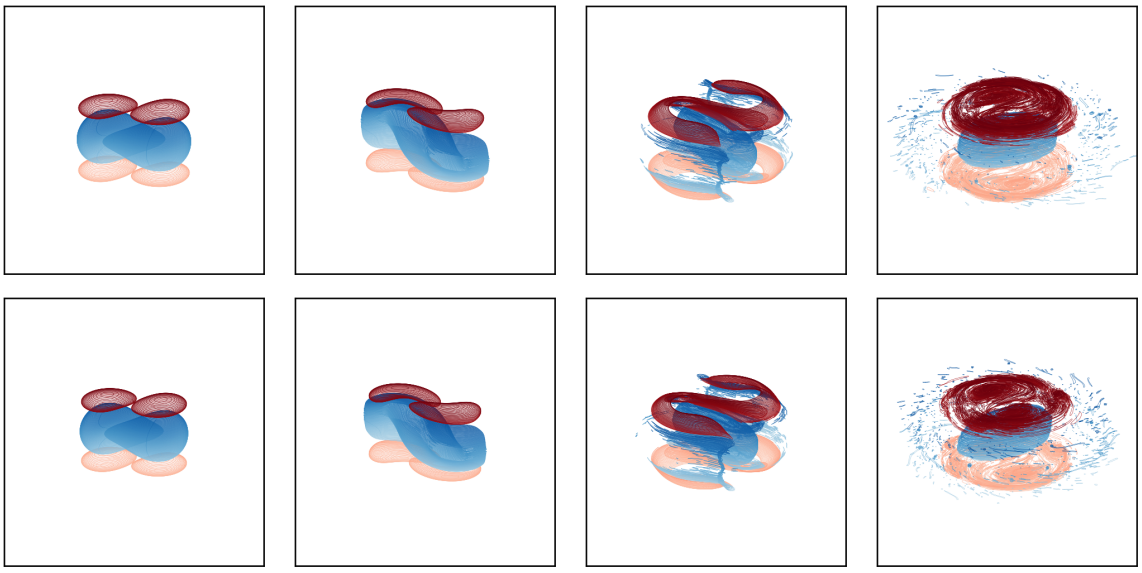

Figure 5. Evolution of the vortex bounding contours for two interacting baroclinic, tripolar eddies for $\Delta x/r_h = 2.1$, and from left to right at $t = 1$, 3, 10, and 200. First row: $\Delta z = 0$ and the eddies are asymmetric. Second row: $\Delta z = 0$, and the eddies are symmetric. The contours are viewed orthographically at an angle of 65° from the vertical axis. The colour shading indicates the depth z of the contours, with lighter contours near the bottom. Red contours bound positive (cyclonic) PV, blue contours bound negative (anticyclonic) PV (Colour online).

after the interaction.

Then, as Δx increases, the volume ratio V_f/V_0 for the largest anticyclone decreases continuously, and reaches values less than but close to 1, when $\Delta x \gtrsim 2.65$ for the symmetric case and $\Delta x \gtrsim 2.7$ for the asymmetric case. For such large horizontal offsets, the largest vortex overall loses material rather than gains some. The material lost is however small. For intermediate horizontal offsets, $2.5 \lesssim \Delta x/r_h \lesssim 2.75$, the second largest anticyclone retains a non-negligible fraction of its initial volume. This indicates that the two vortices merge to create a larger structure which eventually breaks asymmetrically into two unequal-sized vortices.

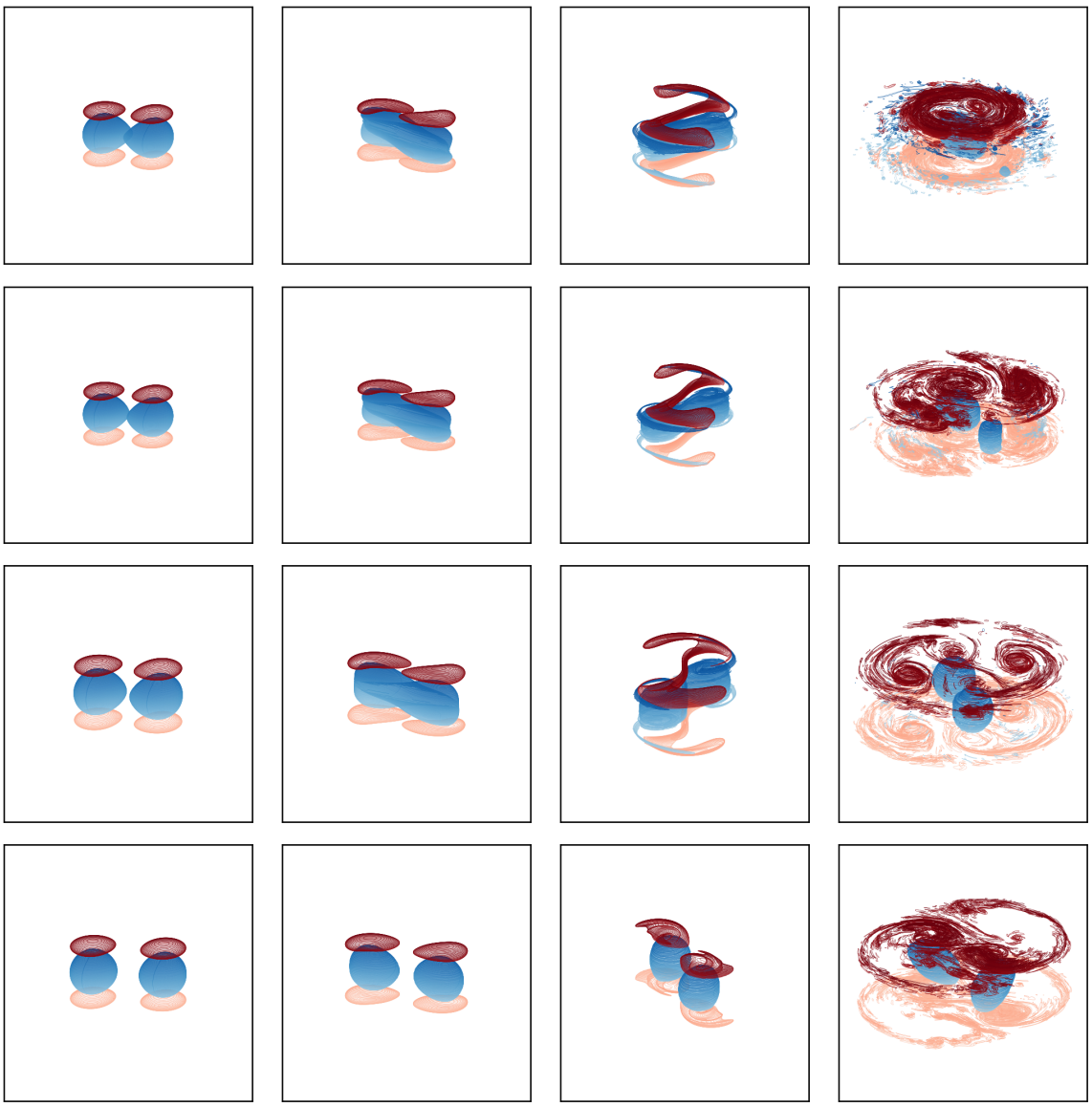

Figure 6. Evolution of the vortex bounding contours for two symmetric interacting baroclinic, tripolar eddies for $\Delta z = 0$ at, from left to right, $t = 1$, 3, 10, and 200. First row: $\Delta x/r_h = 2.5$. Second row: $\Delta x/r_h = 2.6$. Third row: $\Delta x/r_h = 2.7$. Fourth row: $\Delta x/r_h = 3.2$. The contours are viewed orthographically at an angle of 65° from the vertical axis. The colour shading indicates the depth z of the contours, with lighter contours near the bottom. Red contours bound positive (cyclonic) PV, blue contours bound negative (anticyclonic) PV (Colour online).

For large horizontal offsets, the volumes of the two second largest anticyclones are comparable, confirming that the interaction between the two vortices is weak.

Figure 6 shows the interaction of the two tripolar eddies for increasing values of the horizontal offset $\Delta x/r_h = 2.5$, 2.6, 2.7, and 3.2. We can see the continuous transition from a regime where only one large anticyclonic structure forms ($\Delta x/r_h = 2.5$), to one where a secondary anticyclonic satellite forms from the asymmetric splitting of the first merged structure ($\Delta x/r_h = 2.6$), to one where the two anticyclones only periodically touch after an initial short merger, exchanging little material ($\Delta x/r_h = 2.7$) and finally to one where the anticyclones never touch ($\Delta x/r_h = 3.2$). These regimes can be characterised quantitatively. Following Dritschel and Waugh (1992) and Reinaud and Dritschel (2002), we define the merger effi-

ciency for the anticyclones

$$\varrho^-_{eff}(t) = \frac{V^-_{tot}(t) - V^-_{max}(t)}{V^-_{max}(t)} \tag{8}$$

where $V^-_{tot}(t)$ is the total volume of negative PV present in the flow at time t and $V^-_{max}(t)$ is the volume of the largest anticyclone. For the binary interaction between two identical vortices, when the vortices first merge, $\varrho^-_{eff} < 0.1$ corresponds to a *complete merger*, $0.1 \leq \varrho^-_{eff} \leq 0.9$ to a *partial merger*, and $\varrho^-_{eff} > 0.9$ corresponds to a *weak exchange*. The interaction is *elastic* when the vortices never touch. Figure 7 shows ϱ^-_{eff} vs $\Delta x/r_h$. The two anticylones completely merge for $\Delta x/r_h \leq 2.55$ for the asymmetric configuration and $\Delta x/r_h \leq 2.5$ for the symmetric configuration. Recall that the anticyclones are subject to a slightly more intense shear from the cyclonic lenses in the symmetric case. The interaction is a partial merger for $2.6 \leq \Delta x/r_h \leq 2.65$ for the asymmetric case and $2.55 \leq \Delta x/r_h \leq 2.6$ for the symmetric case. For larger horizontal offsets the interaction is either a weak exchange or an elastic interaction. The thresholds separating the different regimes of interaction are consistent with the ones obtained by Reinaud and Dritschel (2002) for the merger of two spherical monopolar eddies. Reinaud and Dritschel (2002) showed that for $\Delta z = 0$, complete merger occurred for $\Delta x/r_h \leq 2.55$, partial merger for $2.6 \leq \Delta x/r_h \leq 2.7$, weak exchange and elastic interactions for $\Delta x/r_h \geq 2.75$. It should however be noted that Reinaud and Dritschel (2002) used a tri-periodic hybrid Eulerian-Lagrangian method (the Contour Advective Semi-Lagrangian method, introduced by Dritschel and Ambaum (1997), and the vortices were typically mapped by fewer horizontal layers. This means that the presence of the upper and lower cyclonic lenses has a relatively weak qualitative influence on the nature of the interaction for the central anticyclonic vortices. It should however be noted that this may not be true beyond the QG regime, when ageostrophic effects are no longer small and must be taken into account. Indeed, although there is no dynamical asymmetry between cyclonic and anticyclonic vortices under the QG approximation, cyclones and anticylones have different properties at finite Rossby numbers. Cyclones tend, in general, to be more stable than anticylones, see Tsang and Dritschel (2015). Moreover, the study of the merger of two monopolar vortices at finite Froude and Rossby number by Reinaud and Dritschel (2018) has shown the strong influence of vertical shear on the strong interaction. Anticyclonic vortices appear to be more sensitive to vertical shear than cyclonic vortices. These effects are likely to affect the evolution of a pair of interacting baroclinic tripoles, where the multipolar nature of the interaction provides additional sources of vertical shear.

Figure 8 shows the time evolution of the distance δx between the centroids of the two largest anticyclones in the flow. Merger is seen through a drop of this distance to zero when only one anticyclonic vortex is present. Merger occurs when $\Delta x/r_h \leq 3$. As expected merger happens sooner if the vortices are initially closer. Then a secondary vortex detached and δx increases. Note that δx may exceed its initial value. This may happen when the two main structures have different volume.

Figure 9 shows the initial and final distributions of volume of PV as a function of the characteristic length scale r, based on the volume, for $\Delta z = 0$ and $\Delta x/r_h = 2.1$, 2.4, 2.7 and 3.1 for symmetric cases. To that purpose we first define $r_{max} = \sqrt[3]{2}\, r_h \simeq 1.26\, r_h$, the mean radius of a vortex twice the size of the initial anticyclones. This corresponds to the largest possible vortex in the flow, hypothetically produced by the full merger of the two anticyclones. We then divide the range $[0, r_{max}]$ into 20 *bins* of equal width $r_{max}/20$ and we accumulate the volumes of all structures present in the flow in the bin corresponding to the mean radius r of the structure. The mean radius is, by definition, the radius of a sphere of the same volume. For a contiguous region of PV of volume V, $r \equiv \sqrt[3]{3V/(4\pi)}$. Initially all the volume is contained in two separate scales: $r_h \simeq 0.8\, r_{max}$ for the spherical anticyclones and $\sqrt[3]{1/4}\, r_h \simeq 0.5\, r_{max}$

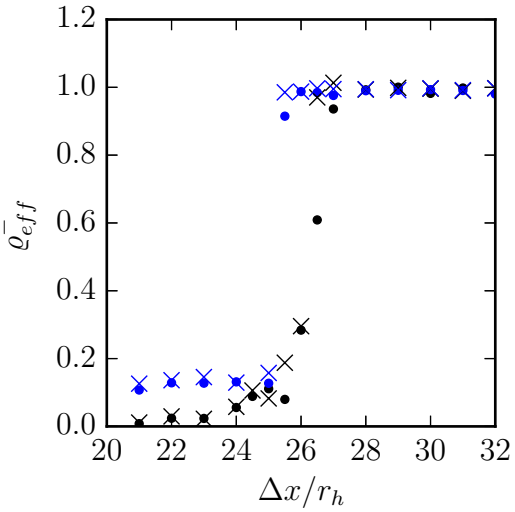

Figure 7. Merger efficiency for the central anticyclones $\varrho^-_{eff} = (V^-_{tot} - V^-_{max})/V^-_{max}$ at $t = 200$, for $\Delta z/r_h = 0$ (black) and $\Delta z/r_h = 1.25$ (blue). •: asymmetric baroclinic tripolar eddies, ×: symmetric baroclinic tripolar eddies (Colour online).

for the cyclonic lenses. The associated volumes are indicated by the black bars in figure 9. At the final time, $t = 200$, some PV volume (red bars in figure 9) has been transferred to small scales in all four cases. For $\Delta x/r_h = 2.1$ and 2.4, the two anticyclones partially merge. This results in a transfer of volume of PV to larger scales. This transfer increases with the merger efficiency discussed above. There is no merger for $\Delta x/r_h = 3.1$ and only weak exchange for $\Delta x/r_h = 2.7$. This results in no creation of larger scale, and only a diminution of the volume present at the scale r_h by filamentation of the two anticyclones. For $\Delta x/r_h = 2.7$, the cyclonic vortices also partially survive (see the second largest red bar of the third panel of figure 9 for $20r/r_{max} = 7$). In this case the two sets of cyclones initially merge but two (upper and lower) cyclonic merged structures break apart. Two main cyclones emerge from the splitting, move away from the other vortices and manage to withstand the shear induced by the other vortices.

For a small vertical offset, $\Delta z/r_h = 1.25$, the situation is different. The final volume of the largest anticyclone varies little with the horizontal distance Δx if $\Delta x/r_h \lesssim 2.5$. In these cases $V_f \simeq 1.4V_0$, see figure 4(a). The two anticyclonic vortices first merge to create an unstable tilted dumbbell-like structure. This structure eventually breaks symmetrically into two main unequal-sized vortices and a plethora of filaments and small scale debris. The final volume of the largest vortex is typically less than the volume of the largest vortex for the same horizontal offset but $\Delta z = 0$. This is first expected because horizontally-aligned anticyclones ($\Delta z = 0$) are overall closer together than vertically shifted anticyclones ($\Delta z \neq 0$) for a given Δx. But this alone cannot explain the difference. In the case $\Delta z = 0$, the vortices occupy the same range of depths, hence they can potentially merge over a wider depth range than vertically-offset vortices can. Recall indeed that the lack of vertical advection implies that only PV regions at the same vertical level can merge. Horizontally-aligned vortices create a stronger link and exchange more material during the early stages of the merger than vertically-offset vortices do. Moreover, the titled dumbbell structure first formed during the merger of two vertically-offset vortices is more deformed and less compact than the dumbbell structure formed for $\Delta z = 0$. The former is more sensitive than the latter to both the self-induced shear and the shear and strain induced by the surrounding cyclonic PV.

For largest horizontal offsets, the vortices are too far apart to strongly interact. The two anticyclones only shed a limited amount of material as attested by the $V_f/V_0 \lesssim 1$ for the two

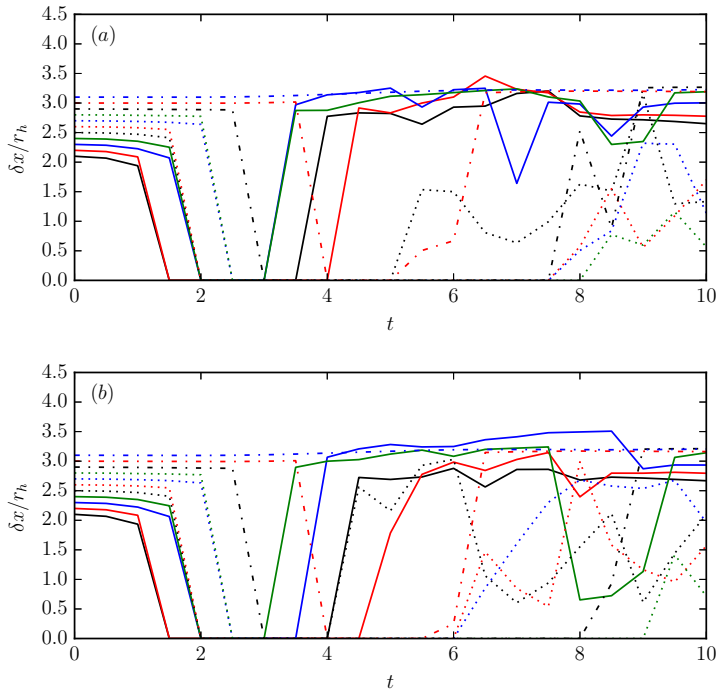

Figure 8. Horizontal distance δx between the two largest anticyclonic vortices for $\Delta z = 0$ and (a) two interacting symmetric baroclinic tripolar eddies and (b) asymmetric baroclinic tripolar eddies. $\Delta x/r_h = 2.1$ (solid black line), 2.2 (solid red line), 2.3 (solid blue line), 2.4 (solid green line), 2.5 (dotted black line), 2.6 (dotted red line), 2.7 (dotted blue line), 2.8 (dotted green line), 2.9 (dash-dotted black line), 3.0 (dash-dotted red line), 3.1 (dash-dotted blue line). (Colour online).

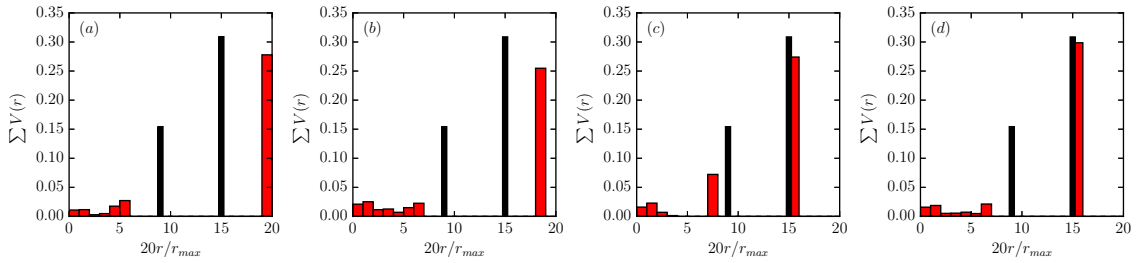

Figure 9. Distribution of the volume of PV contained at the physical scale r for $\Delta z = 0$ and $\Delta x/r_h = 2.1\,(a)$, $2.4\,(b)$, $2.7\,(c)$ and $3.1\,(d)$ at $t = 0$ (black) and $t = 200$ (red) for symmetric cases (Colour online).

largest anticyclonic structures in figure 4.

Figure 10 shows the interaction between symmetric eddies for $\Delta z/r_h = 1.25$ and $\Delta x/r_h = 2.1$, 2.5, 2.8. $\Delta x/r_h = 2.1$ is the smallest horizontal offset tested while $\Delta x/r_h = 2.5$ corresponds to the largest horizontal offset for which the anticyclones partially merge as shown in figure 7. In both cases, we observe the formation of a larger, persistent structure as a result of the merger. For $\Delta x/r_h = 2.6$ and 2.7 (not shown) the two central anticyclone merge at early stage but detach rapidly almost symmetrically. Figure 4 confirms that, in both these cases, at the end of the simulation the two largest anticyclones have nearly equal volumes, also close to their initial volume. For $\Delta x/r_h \geq 2.8$, shown in figure 10 (third row), the two anticyclones never touch.

For $\Delta z/r_h = 2.5$ the two anticyclones are vertically disjoint and cannot merge. They can however shed material due to the shear induced by the vortices. For all values of Δx investigated, the amount of material shed by the two anticyclones is small and the vortices retain

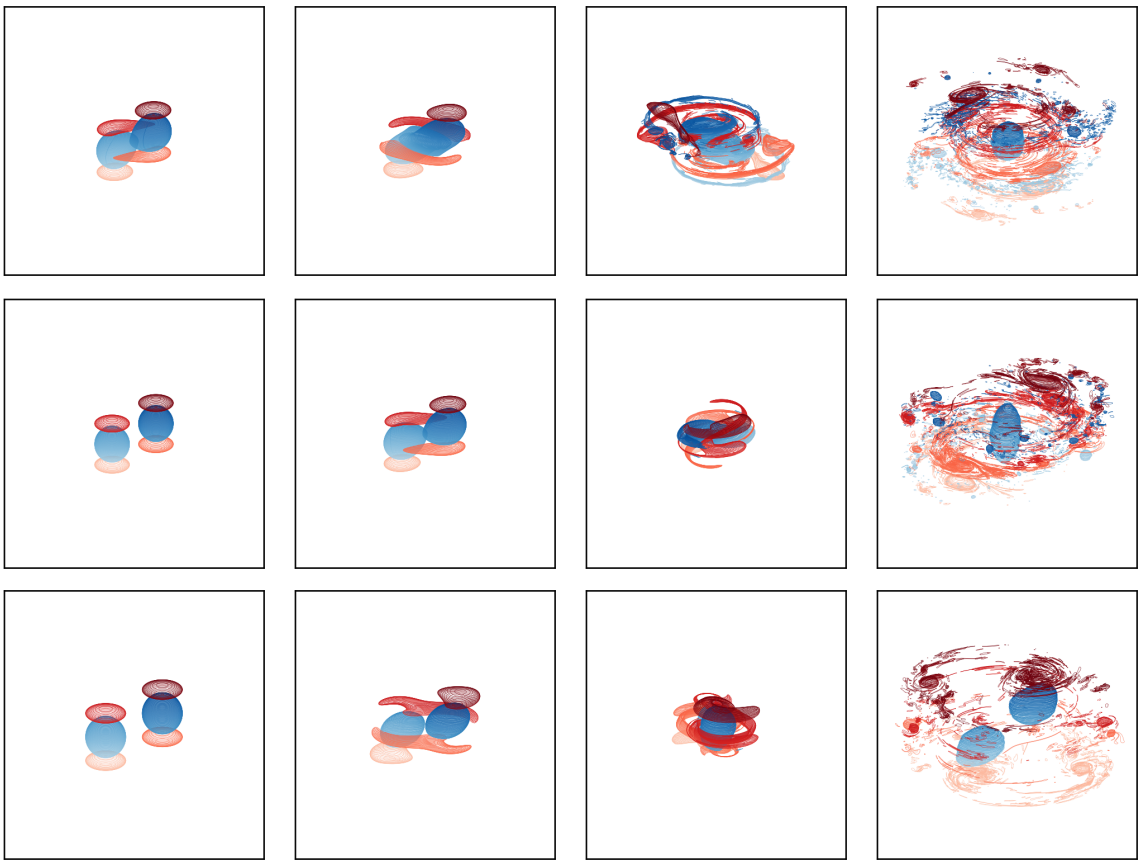

Figure 10. Evolution of the vortex bounding contours for two interacting baroclinic, symmetric tripolar eddies for $\Delta z/r_h = 1.25$. First row: $\Delta x/r_h = 2.1$ and from left to right at $t = 1$, 3, 34, and 200. Second row: $\Delta x/r_h = 2.5$ and $t = 0$, 2, 11.5, 200. Third row: $\Delta x/r_h = 2.8$ and $t = 0$, 5, 12, 200. The contours are viewed orthographically at an angle of 65° from the vertical axis. The colour shading indicates the depth z of the contours, with lighter contours near the bottom. Red contours bound positive (cyclonic) PV, blue contours bound negative (anticyclonic) PV (Colour online).

most of their PV. Figure 11 shows the evolution of the two tripolar eddies for $\Delta x/r_h = 2.1$ and $\Delta x/r_h = 3.1$. The two central anticyclones deform little.

It should be noted however that in all cases, even when the two anticyclones are little affected by the interaction, the cyclonic lenses always experience strong deformation and are often strained out.

We next conduct a similar analysis for the four largest cyclonic eddies present in the flow at the end of the simulation. The ratio of the final volume to their initial volume, V_f/V_0, for these cyclonic vortices is presented in figure 12. The evolution of the cyclonic lenses is more complex than the evolution of the central anticyclones. Their PV is, in absolute value, less than the one of the anticyclones, and they are easily strained out by the anticyclones.

For $\Delta z = 0$ both lower (resp. upper) lenses of each tripolar eddy are at the same vertical level. For all horizontal distance considered in the paper, $2.1 \leq \Delta x/r_h \leqq 3.2$, the lenses deform strongly and merge, even if only temporarily, at some point during the simulation. There is a competition between the horizontal shear and vertical shear, mainly exerted by the large anticyclones, and the ability of the cyclonic lenses to merge and hence to form a large cyclonic vortex. If Δx small, the lower (resp. upper) cyclonic lenses of the two eddies first merge together rapidly. The structure breaks slightly asymmetrically. By the end of the simulation, the resulting structures are however typically smaller in volume than the initial lenses (except for the asymmetric case with $\Delta x/r_h = 2.4$). This is due to the fact that the low-PV cyclonic vortices are subjected to an intense shear and strain from the anticyclones

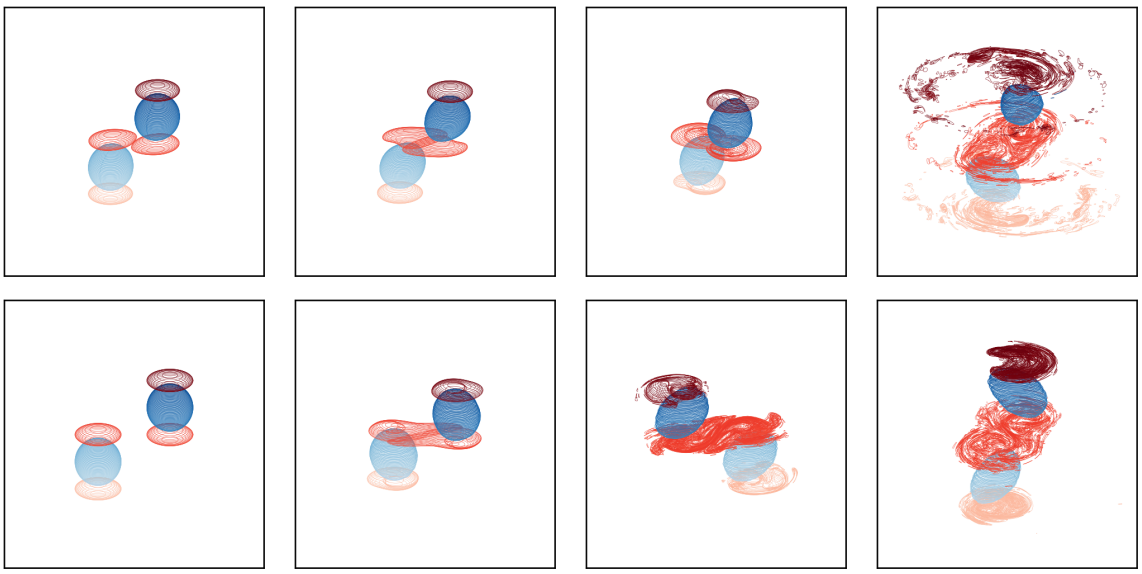

Figure 11. Evolution of the vortex bounding contours for two interacting baroclinic, symmetric tripolar eddies for $\Delta z/r_h = 2.5$. First row: $\Delta x/r_h = 2.1$, and from left to right at $t = 1$, 3, 10, and 200. Second row: $\Delta x/r_h = 3.1$ and $t = 0$, 9.5, 52.5, and 200. The contours are viewed orthographically at an angle of 65° from the vertical axis. The colour shading indicates the depth z of the contours, with lighter contours near the bottom. Red contours bound positive (cyclonic) PV, blue contours bound negative (anticyclonic) PV (Colour online).

and loses large amounts of material to large spiralling filaments. This can be seen in figure 6. Additionally, figure 13 (left) shows a top view on the horizontal layers occupied by the largest cyclonic vortex at $t = 200$. We see two main compact vortices surrounded by a ring of filamentary PV.

For larger horizontal offsets the interaction between the two eddies is weaker. The lenses located at the same height periodically touch but do not fully merge. All the four lenses are partially strained out by the combination of the vertical shear and horizontal strain induced by the vortices. Large filaments eventually detach from the lenses, decreasing their volume significantly. The evolution of the lenses can also be seen in figure 6.

For $\Delta z/r_h = 1.25$ the situation is different as the four lenses occupy different depths. Merger between the lenses is not possible. The lenses can only lose material. Recall that $\Delta z \equiv x_c^2 - x_c^1 \geq 0$. Hence the overall centre of the tripolar eddy 1 is below the centre of eddy 2. The upper lens of eddy 1 and the lower lens of eddy 2 share common horizontal layers with the central anticyclone of the other eddy. As seen in figure 10, these lenses are rapidly strained around the anticyclonic eddies. The two other cyclonic lenses also later shed long filaments. Figure 14 shows the vertical coordinate of the centre of the four largest cyclones at the end of the simulation, $t = 200$. It shows that the two largest cyclonic vortex at the end of the simulation are the upper lens of the top eddy or the lower lens of the bottom eddy, i.e. the lenses the furthest away from the rest of the PV. These are the ones experiencing the least strain and shear.

The two largest vortices have a larger final volume if Δx is small. This is due to some partial alignment of the positive PV. The vertically outermost cyclonic lenses partially align, during the intermediate stages of the evolution of the interaction, with the cyclonic lenses swirling and wrapping around the anticyclonic eddies. This partial vertical alignment of the deformed cyclonic lenses can be seen in 10 for $\Delta x/r_h = 2.1$ at $t = 34$ (first row, third panel from the left), $\Delta x/r_h = 2.5$ at $t = 11.5$ (second row, third panel from the left), and $\Delta x/r_h = 2.8$ at $t = 12$ (third row, third panel from the left). Recall that for small Δx the anticyclone merge while they do not for large Δx. In the latter case, the innermost lenses are further stretched as

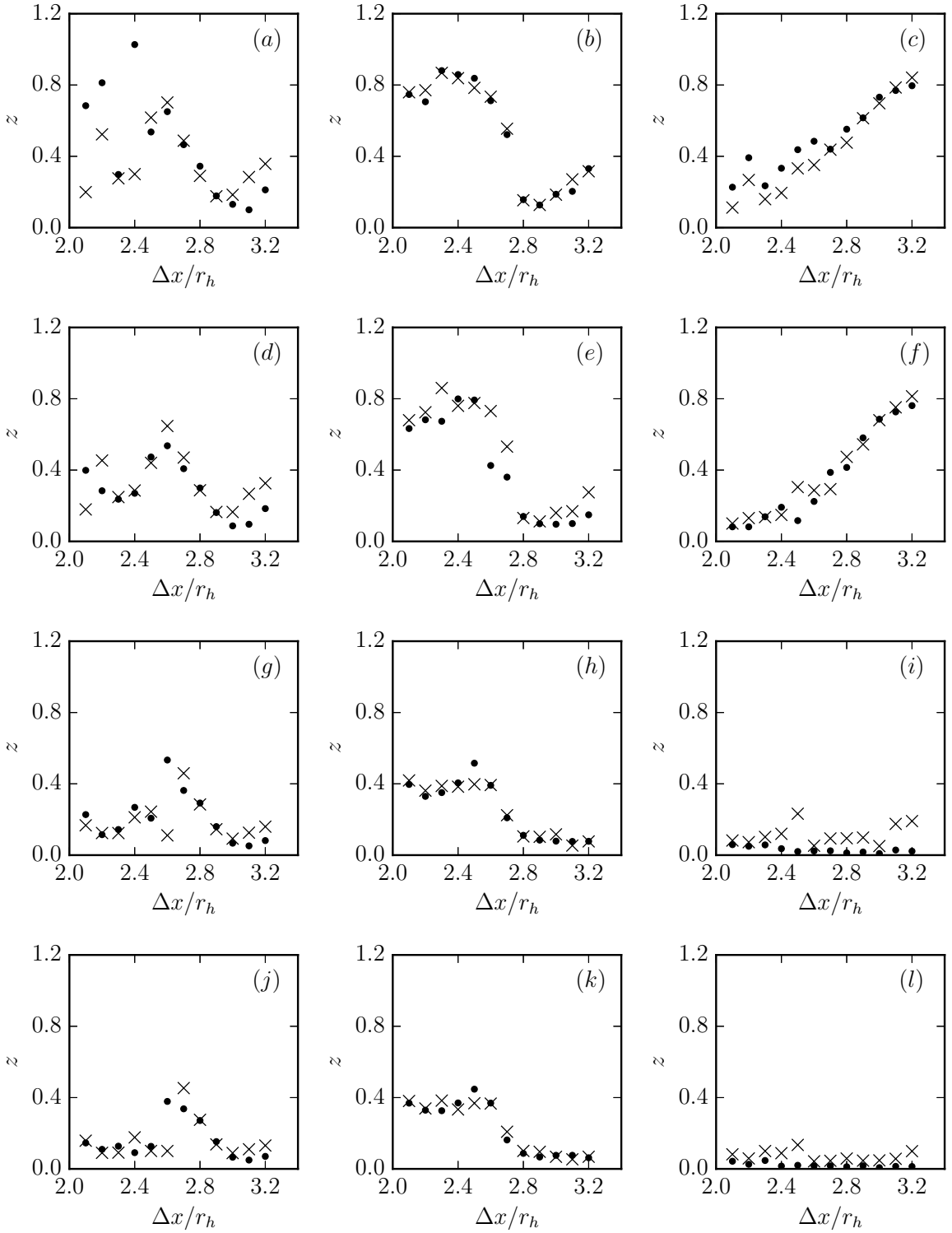

Figure 12. Ratio of the volume V_f at $t = 200$ to the initial volume V_0 for the largest cyclonic vortex present in the flow vs $\Delta x/r_h$ for the asymmetric configuration ($\bullet$) and symmetric configuration ($\times$). The first column of panels corresponds to $\Delta z = 0$, the second column to $\Delta z/r_h = 1.25$, the third column to $\Delta z/r_h = 2.5$. As in figure 12, we rank the first four largest vortices according to their volume. The first row of panels is for the largest vortex (Fi), the second row is for the second largest vortex (Se), the third row is for the third largest vortex (Th) and the fourth row is for the fourth largest vortex (Fo) . Details of the panels in ($\Delta z/r_h$, volume rank) are $(a): (0, Fi)$, $(b): (1.25, Fi)$, $(c): (2.5, Fi)$, $(d): (0, Se)$, $(e): (1.25, Se)$, $(f): (2.5, Se)$, $(g): (0, Th)$, $(h): (1.25, Th)$, $(i): (2.5, Th)$, $(j): (0, Fo)$, $(k): (1.25, Fo)$, $(l): (2.5, Fo)$.

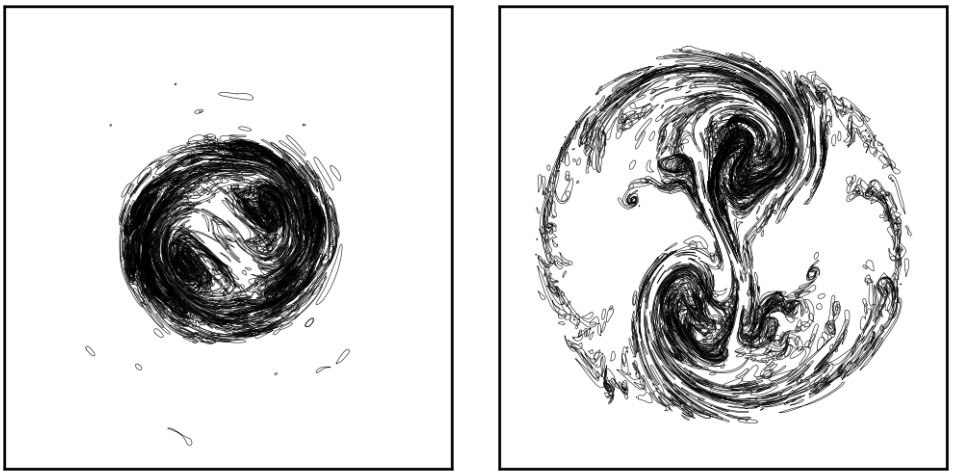

Figure 13. Top view on the vortex bounding contours in the region $(x, y) \in [-1.8, 1.8]^2$ for $\Delta z = 0$ at $t = 200$ for $\Delta x/r_h = 2.2$ (left) and $\Delta x/r_h = 3.1$ (right).

they tend to swirl around both vortices. The outermost lenses, by partially aligning with the innermost lenses are also more stretched and deform if Δx is large. This results in a smaller final main cyclone. The sharp decreases in the volume of the largest cyclone in the graph $V_f/V_(\Delta x)$ is consistent the critical merger distance of the anticyclones in figure 7.

For $\Delta z/r_h = 2.5$, the two innermost lenses, that is the upper lens of eddy 1 and the lower lens of eddy 2 are at the same vertical level and can merge in the symmetric case. Recall that these lenses, containing low PV are strongly deformed by the strain and shear induced by the vortices. The deformation make the innermost vortices merge rapidly. The merged structure is however very deformed and cannot withstand the shear and strain. As a consequence, it is eventually strained out. This can be quantitatively measured by looking at the efficiency of the merger of the two vertically innermost lenses. For that purpose, as a diagnostic of the full simulations, we isolate the horizontal layers which contain the innermost lenses only. We then again identify all coherent structures present in these layers by determining the volumes of contiguous PV. We then calculate the merger efficiency ϱ^+_{eff} defined in a similar way as ϱ^-_{eff} in equation (8) but for the positive PV in these layers. ϱ^+_{eff} is therefore the ratio of the difference between the total volume of positive PV in these layers and the volume of the largest cyclone there, $V^+_{tot}(t) - V^+_{max}(t)$ at time t, to $V^+_{max}(t)$. Results are shown in figure 15. Initially ϱ^+_{eff} equals one for the pair of equal volume lenses. Then, ϱ^+_{eff} collapses to zero as the two lenses merge. The merged vortex sometimes breaks and re-merges while creating small scale debris. However, for all cases, ϱ eventually exceeds the value of 1. This volume of the largest structure is less than half the total volume of PV in these layers: the vortices are small and are being strained out. Indeed $\varrho^+_{eff} > 1$ means $V^+_{tot} > 2V^+_{max}$. Figures 12 and 14 indicate that the largest cyclones at the end of the simulation also stem from the outermost lenses. Again, these are the vortices the furthest away from the rest of the PV. This is true except for the symmetric case for $\Delta x/r_h = 2.1$. In that case, a structure formed by the merger of the two innermost vortices is 10% larger than the second largest vortex, which is located at the top, see figures 12 and 14. It should however be noted that in this case all these cyclonic vortices can in fact seen as debris. Even the largest cyclonic vortex contains, at $t = 200$, only 5% of the initial volume one lens. The fact that the biggest debris are found where the innermost lenses were, may not be significant due to their size. Yet, one can argue that the two innermost lenses are initially very close together, and merge more efficiently than in the other cases for larger Δx. When the merged vortex eventually breaks apart, this large vortex creates larger debris

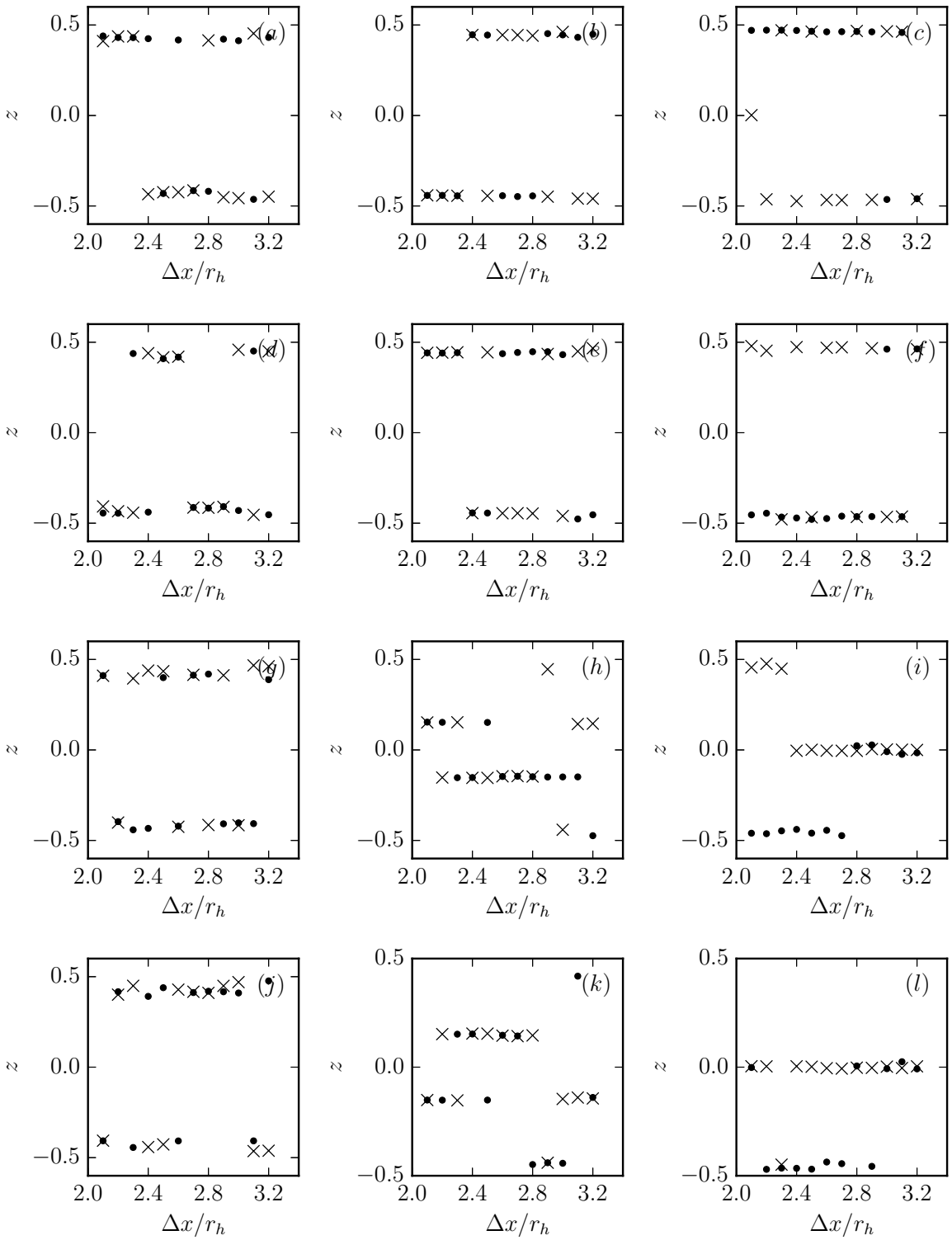

Figure 14. Vertical coordinate of the centre for the cyclonic vortex at $t = 200$ vs $\Delta x/r_h$. The panels are organised as in figure 12.

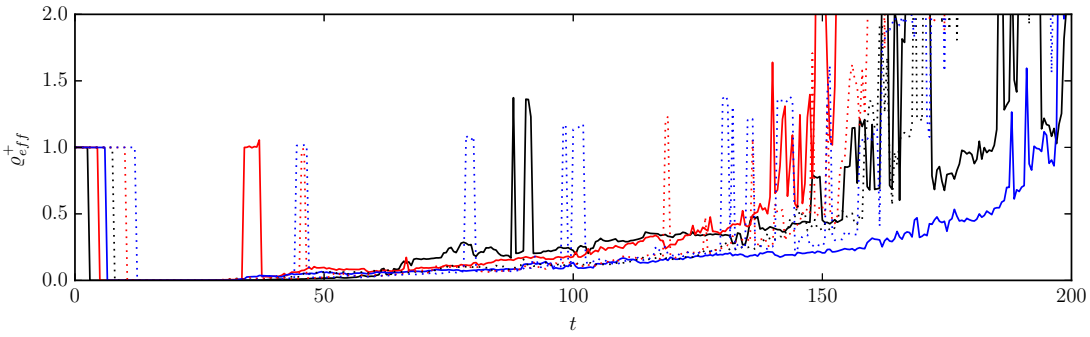

Figure 15. Evolution of the efficiency $\varrho^+_{eff}(t) = (V^+_{tot}(t) - V^+_{max}(t))/V^+_{max}(t)$ for the vertically innermost cyclonic lenses for $\Delta z/r_h = 2.5$. $\Delta x/r_h = 2.1$ (black solid line), 2.3 (red solid line) 2.5 (blue solid line), 2.7 (black dotted line), 2.9 (red dotted line) and 3.1 (blue dotted line). (Colour online).

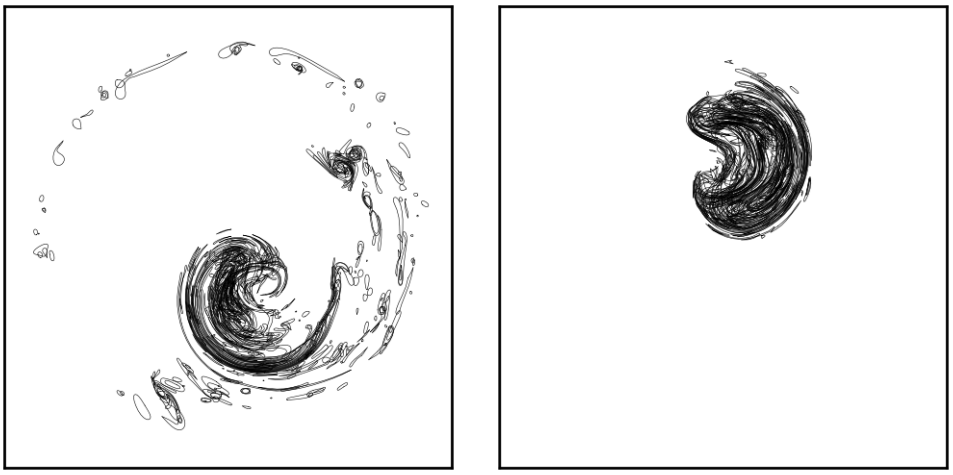

Figure 16. Top view on the vortex bounding contours in the region $(x, y) \in [-1, 1]^2$ for $\Delta z/r_h = 2.5$ at $t = 200$ for $\Delta x/r_h = 2.2$ (left) and $\Delta x/r_h = 3.1$ (right).

compared to the other debris formed from the outermost lenses (which cannot merge with other vortices). For $\Delta x/r_h$ small, all the cyclones are small, see the first column of figure 12. In all cases, all four lenses lose material. The loss of material decreases as Δx increases. This is due to the fact that as Δx increases, these lenses are less influenced by the shear and strain induced by the other tripolar eddy.

Figure 16 provides a top view on the vortex bounding contours in the horizontal layers occupied by the largest cyclonic vortex at $t = 200$ for $\Delta x/r_h = 2.2$ and for $\Delta x/r_h = 3.1$. The lenses have produced more small scale debris and filaments for $\Delta x/r_h = 2.2$ than for $\Delta x/r_h = 3.1$.

4.2. *Alignment of vertically offset eddies*

We next focus on the case $\Delta z/r_h = 3$. This is the case where the two tripolar eddies occupy distinct but contiguous horizontal layers. None of the vortices can merge with another vortex from the other eddy. However, the vortices can still lose material due to the vertical strain and horizontal shear induced by the other vortices. The vortices can also move horizontally. This motion can result in the vertical alignment of the vortices. For example the merger observed by Cresswell (1982) in the East Australian Current can be seen as the result of the alignment

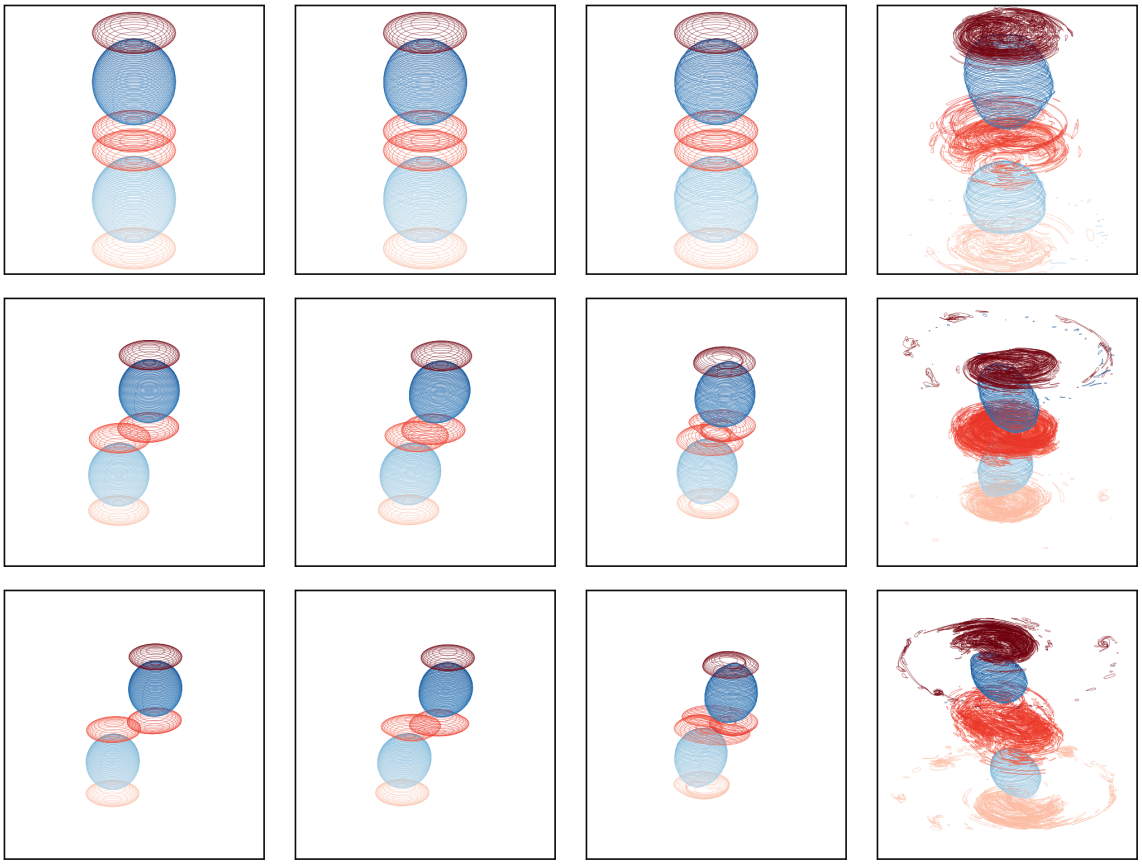

Figure 17. Evolution of the vortex bounding contours for two symmetric interacting baroclinic, tripolar eddies for $\Delta z/r_h = 3$ at, from left to right, $t = 1, 3, 10$, and 200. First row: $\Delta x = 0$. Second row: $\Delta x/r_h = 1$. Third row: $\Delta x/r_h = 1.6$. The contours are viewed orthographically at an angle of 65° from the vertical axis. The colour shading indicates the depth z of the contours, with lighter contours near the bottom. Red contours bound positive (cyclonic) PV, blue contours bound negative (anticyclonic) PV (Colour online).

of the eddies. Vortex alignment is a common occurrence in the oceans.

Most interactions between vertically offset monopolar vortices however does not result in an alignment, as studied recently by the same authors Reinaud and Carton (2020). However the alignment of non-equilibrium or unstable vortices is possible as for example shown experimentally by Hopfinger and van Heijst (1993). For tripolar vortices, the opposite-signed vortices of the tripoles can misalign. This may trigger a relative inward or outward horizontal motion for the vortices.

Figures 17$(a), (b)$ show the evolution of the flow for $\Delta z/r_h = 3$ and $\Delta x/r_h = 0$, 1, and 1.6. We can see that the innermost cyclonic lenses seem to align vertically. They are however subject to a strong vertical shear and horizontal strain and lose a significant amount of material to small scale debris and filament.

Figure 18 shows the evolution of $d^+ = \sqrt{x_m^2 + y_m^2}$ the horizontal distance between the centre (x_m, y_m) of the largest cyclone in the layers initially occupied by the innermost cyclonic lenses and the $z-$axis, as well as the evolution of their volume $V^+(t)$ normalised by the initial volume of a single cyclonic lens $V_\ell^+(0)$ for $\Delta z/r_h = 3$, and $\Delta x/r_h = 0$, 1 and 2.2. The evolution of d^+ provides an indirect indication of alignment of the two innermost cyclonic structures. The process of vertical alignment should be indicated by a decrease in d^+. For $\Delta x = 0$, the two innermost lenses are on the top of each other and therefore touch at $t = 0$. They therefore form a single contiguous structure. It should be noted that, due to the finite discretisation of the lenses, the two vortex bounding contours in contact overlap over a finite area and

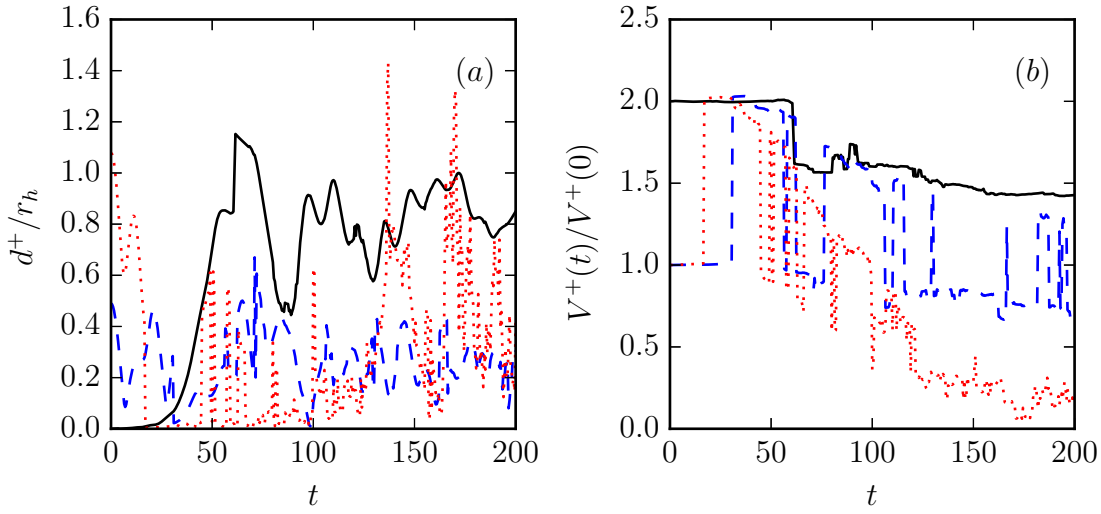

Figure 18. Evolution of (a) the horizontal distance d^+ between the largest innermost cyclone and the z-axis for $\Delta z/r_h = 3$ and $\Delta x/r_h = 0$ (solid balck line), 1 (blue dashed line) and 2.2 (red dotted line), and (b) the relative volume of the largest innermost cyclone $V^+(t)/V^+(0)$ (Colour online).

not just a point. The volume of the connected structure is therefore twice the one of an 'individual' lens of the other cases. This structure partially breaks asymmetrically as seen from the sharp decrease in its volume at $t \simeq 62$, and further sheds debris and filaments as the flow evolves. The centre of the largest resulting cyclone moves away from the $z-$axis and is put out of its initial alignment with the other structures. For both $\Delta x/r_h = 1$ and 2.2, despite large amplitude oscillations, due to the complex dynamics and repeated shedding and reattachment of material to the largest cyclonic vortex, the overall trend is that the centre of the main cyclone gets closer to the z-axis. The trend is however small. Moreover, the vortices lose a significant amount of material (see in particular the case $\Delta x/r_h = 2.2$), reducing the pertinence of attempting to quantify the alignment of the lenses.

We next focus on the two main vortices: the two central anticyclones. We denote $\delta x(t)$ (resp. δz) the time dependent horizontal (resp. vertical) separation between the centres of the two largest anticyclones. It should be noted that $\delta x(0) = \Delta x$, and $\delta z(0) = \Delta z$. Figure 19 shows evolution of $\phi(t) = \tan^{-1}(\delta z(t)/\delta x(t))$ for $0 \leq \Delta x/r_h \leq 2.2$ with an increment of 0.1 between cases. If the two vortex centres aligned vertically ($\delta x \to 0$) then $\phi \to \pi/2$. Results show that the angle ϕ oscillates but does not increase by the end of the simulation from its initial value in almost all cases. There is no tendency to alignment for the anticyclones. In fact for intermediate values of Δx the angle tend to decrease, indicating that δx has increased. Figures 17(c), (d) shows the ratio $\phi(200)/\phi(0)$, confirming that for intermediate values of Δx the anticyclones move further away from vertical alignment. The decrease in angle remains very small, 5% at most.

5. Isolated tripolar eddies

In the previous sections, we have focused on tripolar eddies for which the lower and upper cyclonic lenses carry little strength compared to the central anticyclone. This regime is relevant to Meddies. Significant differences are expected if the cyclonic lenses have strengths comparable to the strength of the central anticyclones. Of particular interest are the so-called isolated eddies whose overall strength vanishes. In this case, the far field induced by the eddies is very weak. We therefore consider the interaction between two symmetric eddies, with the

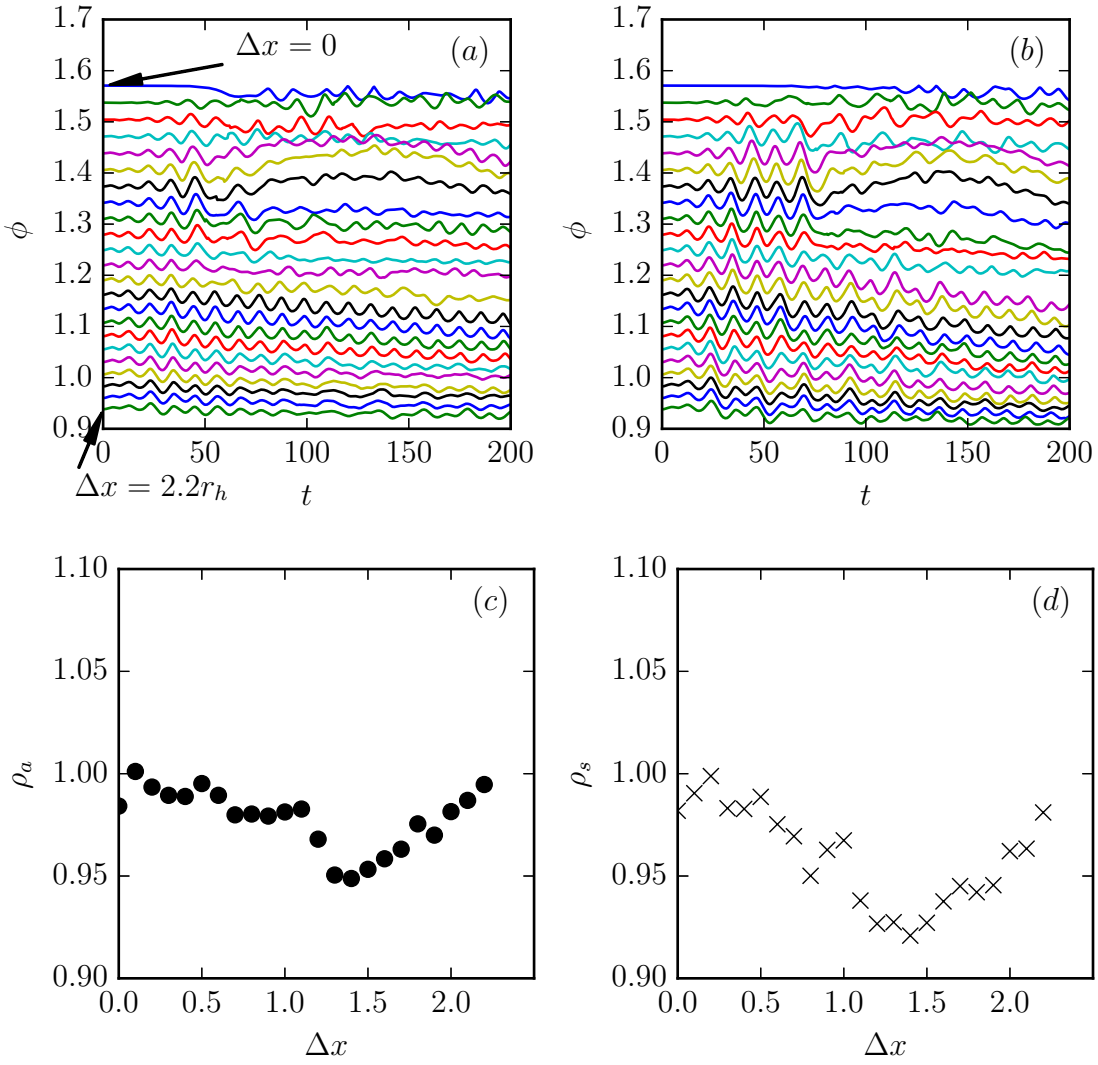

Figure 19. Evolution of the tilt angle $\phi(t) = \tan^{-1}(\delta z(t)/\delta x(t))$ for $\Delta z/r_h = 3$, and $0 \leq \Delta x/r_h \leq 2.2$ and for (a) the asymmetric configurations and (b) the symmetric configurations. $\Delta x/r_h$ varies by 0.1 between consecutive curves. Ratio $\phi(200)/\phi(0)$ vs Δx for (c) the asymmetric configurations and (d) the symmetric configurations (Colour online).

same geometry as before, but with $q_t = q_b = -2q_c$. Recall that the volume of each lens is a quarter of the volume of the central vortex. This means that the strength of each lens is half, in absolute value, the one of the central vortex. The integrated PV over each tripolar eddy is zero.

We first analyse the linear stability of a single tripolar eddy. The most unstable mode has an azimuthal wave number $m = 2$ with a growth rate $\sigma_r/q_c = 6.948 \times 10^{-2}$. The nonlinear evolution of the unstable eddy is shown in figure 20. We can clearly see the growth of mode $m = 2$ which results eventually in the splitting of each vortex into two main vortices, accompanied small debris. These secondary vortices form secondary tripolar vortices. The vortices of these secondary tripolar eddies are not vertically aligned and have a dipolar moment which makes them move away from each other. Again, this is similar to hetons breaking as the result of the growth of an azimuthal mode $m = 2$.

Figure 21 shows the evolution of the two isolated eddies for $\Delta z = 0$ and $\Delta x/r_h = 2.2$. During the early evolution of the flow, the lenses and the central vortices of the two eddies merge. However, due to baroclinic effects, the cyclonic and anticyclonic vortices move away from

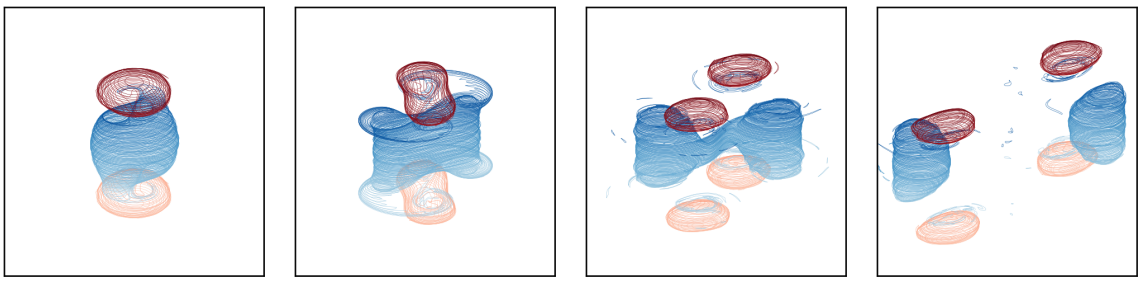

Figure 20. Evolution of the vortex bounding contours for a singlesymmetric, isolated baroclinic, tripolar eddy from left to right, $t = 24$, 35, 51, and 62. The contours are viewed orthographically at an angle of 65° from the vertical axis. The colour shading indicates the depth z of the contours, with lighter contours near the bottom. Red contours bound positive (cyclonic) PV, blue contours bound negative (anticyclonic) PV (Colour online).

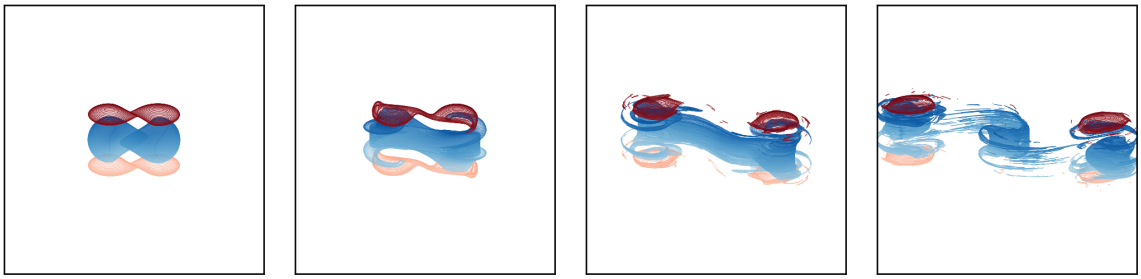

Figure 21. Evolution of the vortex bounding contours for two symmetric, isolated baroclinic, tripolar eddies for $\Delta z = 0$ and $\Delta x/r_h = 2.2$ at, from left to right, $t = 1$, 4, 10, and 17. The contours are viewed orthographically at an angle of 65° from the vertical axis. The colour shading indicates the depth z of the contours, with lighter contours near the bottom. Red contours bound positive (cyclonic) PV, blue contours bound negative (anticyclonic) PV (Colour online).

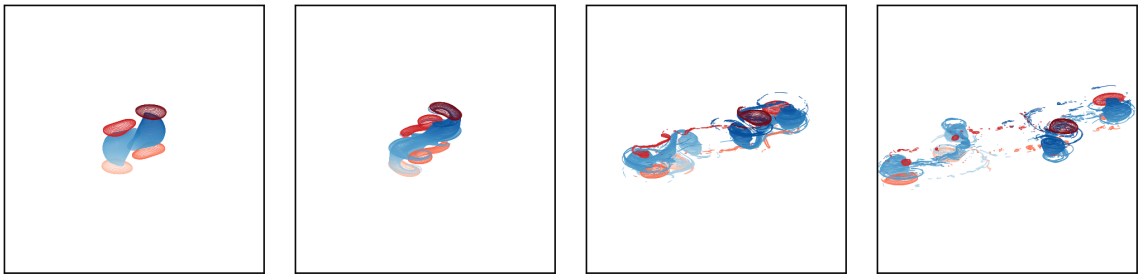

Figure 22. Evolution of the vortex bounding contours for two symmetric, isolated baroclinic, tripolar eddies for $\Delta z/r_h = 1.25$ and $\Delta x/r_h = 2.2$ at, from left to right, $t = 2$, 5.5, 20 and 30. The contours are viewed orthographically at an angle of 65° from the vertical axis. The colour shading indicates the depth z of the contours, with lighter contours near the bottom. Red contours bound positive (cyclonic) PV, blue contours bound negative (anticyclonic) PV (Colour online).

vertical alignment, creating a dipolar moment. The merged structure is pulled apart. Two misaligned tripolar eddies move away from the centre of the domain. A bridge of negative PV has formed between the two anticylones. This bridge is stretched by the tripolar vortices moving away from the centre of the domain. This stretching is not intense enough to stabilise the bridge of PV which eventually rolls up, creating a small cyclonic structure in the centre. By symmetry, this vortex remains near the centre, at least until the end of the simulation $t = 20.5$. It should be noticed that the evolution the flow after the initial merger of the eddies is similar to the evolution of unstable hetons, see Reinaud and Carton (2009).

We conduct a similar numerical experiment for $\Delta z/r_h = 1.25$. Results are shown in figure 22. The situation is more complex. Recall that for $\Delta z/r_h = 1.25$ the cyclonic lenses cannot merge. The two anticyclones first merge to form a tilted dumbbell-like structure. Each part of the

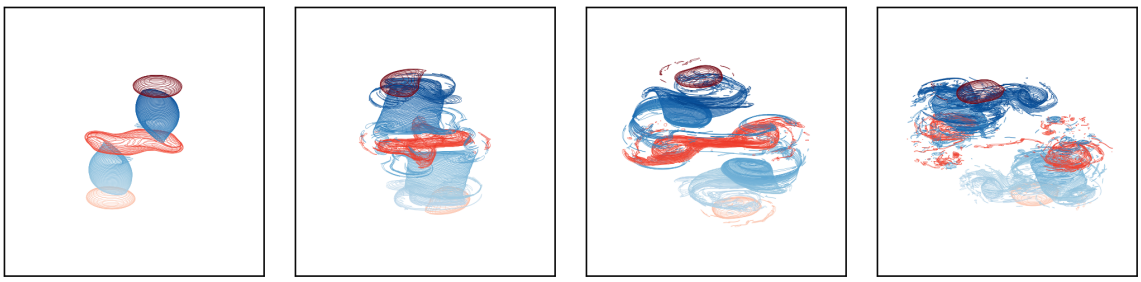

Figure 23. Evolution of the vortex bounding contours for two symmetric, isolated baroclinic, tripolar eddies for $\Delta z/r_h = 2.5$ and $\Delta x/r_h = 2.2$ at, from left to right, $t = 3$, 14, 22.5 and 34.5. The contours are viewed orthographically at an angle of 65° from the vertical axis. The colour shading indicates the depth z of the contours, with lighter contours near the bottom. Red contours bound positive (cyclonic) PV, blue contours bound negative (anticyclonic) PV (Colour online).

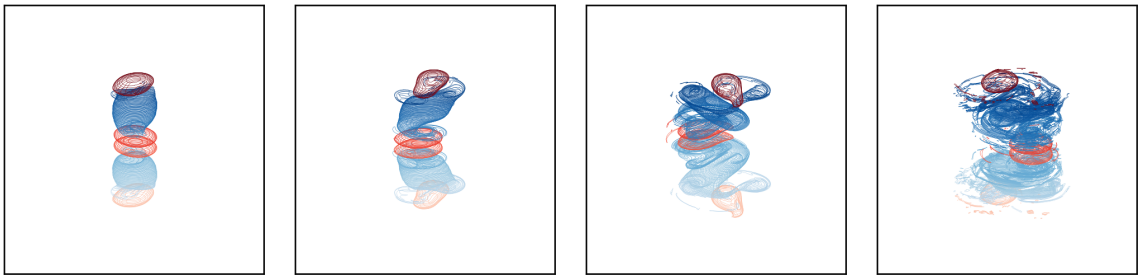

Figure 24. Evolution of the vortex bounding contours for two symmetric, isolated baroclinic, tripolar eddies for $\Delta z/r_h = 3$ and $\Delta x/r_h = 0$ at, from left to right, $t = 15.5$, 20.5, 27.5 and 44. The contours are viewed orthographically at an angle of 65° from the vertical axis. The colour shading indicates the depth z of the contours, with lighter contours near the bottom. Red contours bound positive (cyclonic) PV, blue contours bound negative (anticyclonic) PV (Colour online).

dumbbell-like structure strongly interact with the innermost cyclonic lenses. The strain and shear induced by the upper lens of the lower tripolar eddy shears and splits the anticyclonic central vortex of the upper tripolar eddy in two main vortices. So does the lower lens of the upper eddy to the central cyclone of the lower eddy. At the same time, the upper lense of the upper eddy moves out of alignment with the anticyclone of the same eddy, creating a dipolar moment as for the case $\Delta z = 0$.

Consequently, the first main vortex resulting from the splitting of the central anticyclone of the upper eddy, eddy 2, pairs with its the upper cyclonic lens and moves away from the centre of the domain as a heton. Meanwhile the second main part of the same anticyclone pairs with the upper lens of the lower eddy, eddy 1, as a dipole which also moves away from the centre of the domain. The fate of the second anticyclone is similar.

For $\Delta z/r_h = 2.5$ and $\Delta x/r_h = 2.1$ the two innermost lenses merge rapidly as can be seen in figure 23. The merged lens eventually breaks into two secondary vortices as it is pulled apart by the heton-like structures formed by the misaligned central anticyclones and cyclonic outermost lenses. Eventually the structures form highly deformed secondary multipolar structures which move away from each other.

Finally for $\Delta z/r_h = 3$ and $\Delta x = 0$, the situation is different. Results are shown in figure 24. The two innermost lenses remain vertically aligned during the duration of the simulation $t \in [0, 35]$, but move away from the $z-$axis. The other vortices are put out of alignment with the innermost lenses. The symmetry of the flow with respect to the horizontal plane passing between the two innermost lenses is preserved and all vortices remain near the centre of the domain, at least until $t = 35$. The two anticyclones deform and partially break due to the intense shear and strain induced by the cyclonic lenses.

6. Conclusions and perspectives

We have explored the interaction between two tripolar baroclinic eddies. Considered separately each eddy is only weakly unstable. The instability puts the vortices out of alignment. The resulting increased vertical shear and horizontal strain leads to the partial break-up of the small, low PV, upper and lower lenses surrounding the high-PV large anticyclone.

In the case of two interacting eddies, the two central anticyclones merge together provided they are closer than a threshold. This threshold is roughly the same as the one obtained for the same vortices without the upper and lower lenses. This is not surprising, considering the difference in strength between the central vortices and the lenses (between 13.3 and 20 as indicated in section 2). In general the lenses are partially destroyed during the interaction, generating large amounts of small scale debris and filament.s These further feed the energy and enstrophy cascades.

Similarly to the study of the alignment between two monopolar vortices by Reinaud and Carton (2020), the tripolar eddies do not strongly align vertically by themselves. Again, the efficient alignment of such structures requires an additional external velocity field pushing the two structures closer together.

The current study was performed under the quasi-geostrophic approximation in the f-plane. Two natural extensions of this study should be considered. On the one hand, in practice, the interaction between such meso-scale eddies occurs over a relatively large horizontal area. Hence, an extension of this work in the $\beta-$plane, where the effects of the natural background variation of the planetary vertical vorticity are taken into account, at leading order, could be considered. This background planetary vorticity makes vortices drift in a direction depending on the sign of their PV. This differential $\beta-$drift will induce a vertical shear on the baroclinic tripolar vortices. The second natural extension is to consider the ageostrophic effects, by studying the interaction at small yet finite Rossby number. Recent studies by Ciani *et al.* (2016), Reinaud and Dritschel (2018) and Orozco Extrada *et al.* (2020) have shown that these effects can drastically alter the interaction between two vortices, and in particular the way they merge. Notably cyclonic and anticyclonic vortices have asymmetric dynamical behaviours.

Appendix A: Numerical evolution of inviscid invariants

In absence of diffusion, the QG dynamics conserves a collection of invariants: the total energy $\mathcal{E}_{tot} = -\frac{1}{2}\iiint q\varphi \,\mathrm{d}^3\boldsymbol{x}$, the total 'entrophy' $E = \frac{1}{2}\iiint q^2 \,\mathrm{d}^3\boldsymbol{x}$, the angular impulse $J = \frac{1}{2}\iiint q(x^2+y^2)\,\mathrm{d}^2\boldsymbol{x}$ and the linear impulse $\boldsymbol{I} = (I_x, I_y) = \iiint (x,y) q \,\mathrm{d}^3\boldsymbol{x}$. Contour surgery however removes filaments and debris whose scale is less than the surgical scale to control the complexity of the calculation. Surgery mimics the dissipation of the small scales which carry enstrophy cascading to scales below the resolution of the numerical simulation. Figure A1 shows the evolution of the E, I_x and J for the interaction between two symmetric tripolar eddies with $\Delta z = 0$, and $\Delta x/r_h = 2.4$, 3 and 3.2. We see a small decrease of the total volume of PV due to the surgical removal of the debris reaching a size below the surgical scale. This decrease is more important as the tripolar eddies are closer together and their interaction stronger. This decrease in volume has only a small impact of the enstropy, in particular for larger Δx. This is due to the fact that most of the volume lost originates in the low PV cyclonic vortices. Overall, both the linear I_x and angular impulse J are nearly conserved during the interaction.

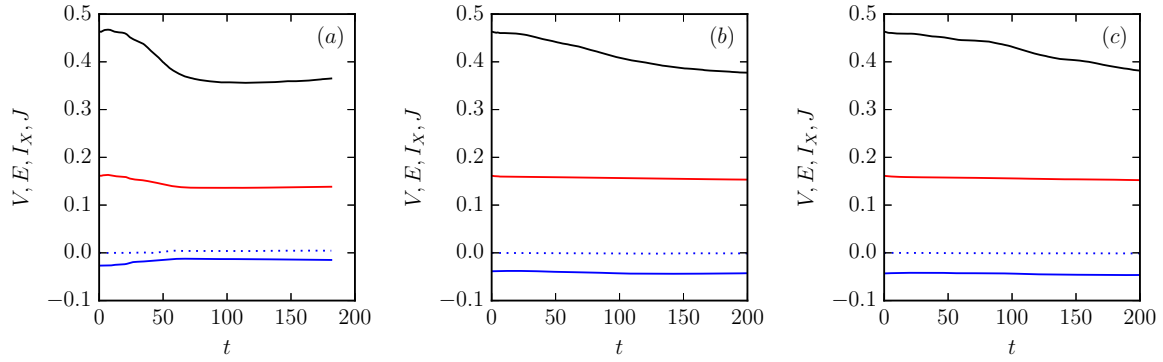

Figure A1. Evolution of the total PV volume V (solid black line), Enstrophy E (solid red line), linear impulse I_x (dotted blue line), and angular impulse J (solid blue line) for the interaction for two symmetric tripolar eddies for $\Delta z = 0$ and (*a*) $\Delta x/r_h = 2.4$, (*b*) 3 and (*c*) 3.2. (Colour online).

References

Bambrey, R.R., Reinaud, J.N. and Dritschel, D.G., Strong interactions between two co-rotating quasi-geostrophic vortices. *J. Fluid Mech.*, 2007, **592**, 117–133.

Bashmachnikov, I. and Carton, X., Surface signature of Mediterranean water eddies in the Northeastern Atlantic: effect of the upper ocean stratification. *Ocean Sci.*, 2012, **8**, 931–943.

Carton, X., Hydrodynamical Modeling of Oceanic Vortices. *Surveys in Geophysics*, 2001, **22**, 179–263.

Carton, X., A., S.M., Menesguen, C., Aguiar, A. and Meunier, T., Vortex stability in a multi-layer quasi-geostrophic model: application to Mediterranean Water eddies. *Fluid Dyn. Res.*, 2014, **46**, 1–18.

Carton, X., Chérubin, L., Paillet, J., Morel, Y., Serpette, A. and Cann, B.L., Meddy coupling with a deep cyclone in the Gulf of Cadiz. *J. Mar. Syst.*, 2002, **32**, 13–42.

Carton, X., Daniault, N., Alves, J., Chérubin, L. and Ambar, I., Meddy dynamics and interaction with neighboring eddies southwest of Portugal : observations and modeling. *J. Geophys. Res.*, 2010, **115**, C06017.

Ciani, D., Carton, X. and Verron, J., On the merger of subsurface isolated vortices. *Geophys. Astrophys. Fluid Dyn.*, 2016, **110**, 23–49.

Cresswell, G., The coalescence of two East Australian Current warm-core rings. *Science*, 1982, **215**, 161–164.

Dijkstra, H., *Dynamical oceanography*, 2008 (Berlin Heidelberg: Springer-Verlag).

Dritschel, D.G., Contour surgery: a topological reconnection scheme for extended integrations using contour dynamics. *J. Comput. Phys.*, 1988, **77**, 240–266.

Dritschel, D.G., A general theory for two-dimensional vortex interactions. *J. Fluid Mech.*, 1995, **293**, 269–303.

Dritschel, D.G., Vortex merger in rotating stratified flows. *J. Fluid Mech.*, 2002, **455**, 83–101.

Dritschel, D.G. and Ambaum, M.H.P., A contour-advective semi-lagrangian algorithm for the simulation of fine-scale conservative fields. *Q. J. R. Met. Soc.*, 1997, **123**, 1097–1130.

Dritschel, D.G. and Saravanan, R., Three-dimensional quasi-geostrophic contour dynamics, with an application to stratospheric vortex dyn amics. *Quart. J. Roy. Meteorol. Soc.*, 1994, **120**, 1267–1297.

Dritschel, D.G. and Waugh, D.W., Qualification of the inelastic interaction of unequal vortices in two-dimensional vortex dynamics. *Phys. Fluids A*, 1992, **4**, 1737–1744.

Hopfinger, E.J. and van Heijst, G.J.F., Vortices in rotating fluids. *Ann. Rev. Fluid Mech.*, 1993, **25**, 241–289.

L'Hégaret, P., Carton, X., Ambar, I., Menesguen, C., Hua, B., Chŕubin, L., Aguiar, A., Cann, B.L., Daniault, N. and Serra, N., Evidence of Mediterranean Water dipole collision in the Gulf of Cadiz. *J. Geophys. Res.*, 2014, **119**, 5337–5359.

Melander, M.V., Zabusky, N.J. and McWilliams, J.C., Symmetric vortex merger in two dimensions: causes and conditions. *J. Fluid Mech.*, 1988, **195**, 303–340.

Menesguen, C., Le Gentil, S., Marchesiello, P. and N., D., Destabilization of an oceanic meddy-like vortex: energy transfers and significance of numerical settings. *J. Phys Oceanogr.*, 2018, **48**, 1151–1168.

Meunier, T., Menesguen, C., X., C., Le Gentil, S. and Schopp, R., Optimal Perturbations of an Oceanic Vortex Lens. *Fluids*, 2018, **3**, 63.

Meunier, T., Menesguen, C.and Schopp, R. and Le Gentil, S., Tracer stirring around a meddy: The formation of layering. *J. Phys. Oceanogr.*, 2015, **45**, 407–423.

Miyazaki, T., Fujiwara, T. and Yamamoto, M., Quasigeostrophic confocal Spheroidal vortices. *J Phys. Soc. Jpn*, 2003, **72**, 2786–2803.

Nguyen, H.Y., Hua, B.L., Schopp, R. and Carton, X., Slow quasi-geostrophic unstable modes of a lens-like vortex in a continuously stratified flow. *Geophys. Astrophys. Fluid Dyn.*, 2012, **106**, 305–319.

Orozco Extrada, A., Cruz Gómez, R.C., Cros, A. and Le Gal, P., Coalescence of lenticular anticlyclons in a linearly stratified rotating fluid. *Geophys. Astrophys. Fluid Dyn.*, 2020, **114**, 504–52.

Overman II, E.A. and Zabusky, N.J., Evolution and merger of isolated vortex structures. *Phys. Fluids*, 1982,

25, 1297–1305.

Ozugurlu, E., Reinaud, J.N. and Dritschel, D.G., Interaction between two quasi-geostrophic vortices of unequal potential-vorticity. *J. Fluid Mech.*, 2008, **597**, 395–414.

Paillet, J., Cann, B.L., Carton, X., Morel, Y. and Serpette, A., Dynamics and evolution of a northern Meddy. *J. Phys. Oceanogr.*, 2002, **32**, 55–79.

Paillet, J., Cann, B.L., Serpette, A., Morel, Y. and Carton, X., Real-time tracking of a northern meddy in 1997-98. *Geophys. Res. Lett.*, 1999, **26**, 1877–1880.

Pingree, R. and Le Cann, B., Structure of a meddy (Bobby 92) southeast of the Azores. *Deep Sea Res. I*, 1993, **40**, 2077–2103.

Reinaud, J.N., Piecewise uniform potential vorticity pancake shielded vortices. *Geophys. Astrophys. Fluid Dyn.*, 2017, **111**, 32–64.

Reinaud, J.N. and Carton, X., The stability and the nonlinear evolution of quasi-geostrophic hetons. *J. Fluid Mech.*, 2009, **636**, 109–135.

Reinaud, J.N. and Carton, X., Existence, stability and formation of baroclinic tripoles in quasi-geostrophic flows. *J. Fluid Mech.*, 2015, **785**, 1–30.

Reinaud, J.N. and Carton, X., The alignment of two three-dimensional quasi-geostrophic vortices. *Geophys. Astrophys. Fluid Dyn.*, 2020, **114**, 524–560.

Reinaud, J.N. and Dritschel, D.G., The merger of vertically offset quasi-geostrophic vortices. *J. Fluid Mech.*, 2002, **469**, 297–315.

Reinaud, J.N. and Dritschel, D.G., The critical merger distance between two co-rotating quasi-geostrophic vortices. *J. Fluid Mech.*, 2005, **522**, 357–381.

Reinaud, J.N. and Dritschel, D.G., The merger of geophysical vortices at finite Rossby and Froude number. *J. Fluid Mech.*, 2018, **848**, 388–410.

Richardson, P.L., Bower, A. and Zenk, W., A census of meddies tracked by floats. *Prog. Oceanogr.*, 2000, **45**, 209–250.

Storer, B., Poulin, F.J. and Menesguen, C., The Dynamics of Quasigeostrophic Lens-Shaped Vortices. *J. Phys. Oceanogr.*, 2018, **48**, 937–957.

Tsang, Y.K. and Dritschel, D., Ellipsoidal vortices in rotating stratified fluids: beyond the quasi-geostrophic approximation. *J. Fluid Mech.*, 2015, **762**, 196–231.

Vallis, G.K., *Atmospheric and oceanic fluid dynamics: fundamentals and large-scale circulation*, 2006 (Cambridge: Cambridge University Press).

von Hardenberg, J., McWilliams, J.C., Provenzale, A., Shchpetkin, A. and Weiss, J.B., Vortex merging in quasi-geostrohic flows. *J. Fluid Mech.*, 2000, **412**, 331–353.

Waugh, D.W., The efficiency of symmetric vortex merger. *Phys. Fluids A*, 1992, **4**, 1745–1758.

Yang, G.B., Zheng, Q., Xiong, X.J., Yuan, Y., Zhuang, Z., Hui, Z., Guo, Y.L., Yu, L., Sun, J., Ju, X., D.-J., M. and Hu, X., Subsurface cyclonic eddies observed in the sourtheastern tropical Indian ocean. *J. Geophys. Res. Oceans*, 2019, **124**.

Yasuda, I., Okuda, K. and Hirai, M., Evolution of a Kurushio warm-core ring - Variability of the hydrographic structure. *Deep-sea Res.*, 1992, **39 (suppl.)**, S131–S161.

Yim, E., Billant, P. and Menesguen, C., Stability of an isolated pancake vortex in continuously stratified-rotating fluids. *J. Fluid Mech.*, 2016, **801**, 508–553.